

***Towards Detection and Retrieval of
Volcanic Ash from SEVIRI
using the OCA Processor***

Final Report

VERSION 1.0

R.Siddans, C. Poulsen

STFC Rutherford Appleton Laboratory
Chilton, Didcot OX11 0QX, U.K.

in response to
EUMETSAT RFQ 10/202688

2 June 2011

Contents

1	Introduction.....	5
2	Background	5
3	Usefulness of individual SEVIRI channels for ash detection and retrieval	6
4	Data-set analysed.....	12
5	Retrieval scheme configuration.....	12
6	Ash Detection with OCA	13
7	Example retrievals along CALISPO orbits.....	16
8	Summary and conclusions.....	19
9	Suggestions for further work	20
10	Supplementary Material	21
11	Collocating CALIPSO data	22
12	References	22

Acronyms

AATSR	Advanced Along-track Scanning Radiometer
AVHRR	Advanced Very High Resolution Radiometer
BT	Brightness temperature
CM	Cloud-model
COT	Cloud optical thickness
CTP	Cloud-top pressure
DU	Dobson Units
ECMWF	European Centre for Medium Range Weather Forecasting
FCI	Flexible Combined Imager
FM	Forward model
IASI	Infrared Atmospheric Sounding Interferometer
ISRF	Instrument spectral response function
LOS	Line-of-sight
LUT	Look-up-table.
LZA	LOS or view zenith angle
MSG	Meteosat Second Generation
MTG	Meteosat Third Generation
NCEO	(UK) National Centre for Earth Observation
OCA	Optimal Cloud Analysis
OE	Optimal estimation
ORAC	Oxford RAL Aerosol and Cloud scheme
RAL	Rutherford Appleton Laboratory
RFM	Reference Forward Model
RT	Radiative transfer
RTTOV	RT model for the Tiros Operational Vertical sounder.
SEVIRI	Spinning Enhanced Visible InfraRed Imager
SZA	Solar zenith angle

1 Introduction

The following report describes work carried out in response to Eumetsat RFQ No. 10/202688 “Towards Detection and Retrieval of Volcanic Ash from SEVIRI using the OCA Processor”

Three points are addressed by the work conducted here:

1. The usefulness of the individual SEVIRI channels for retrieval of ash is considered, with particular emphasis on plume altitude, optical depth and scene discrimination.
2. Options for SEVIRI volcanic ash detection are considered with particular reference to OCA framework and with regard to operational implementation
3. Examples of SEVIRI retrievals for the Eyjafjallajokull case are provided, with validation of retrieved height against CALIPSO observations.

2 Background

The detection and retrieval of properties of volcanic ash by geostationary satellites could be an important tool for warnings and information to aviation in the event of a significant eruption. Basic ash properties available from the SEVIRI imager data should include the ash altitude, optical depth and columnar mass. All quantities could be important in the advisability of flying commercial aircraft through airspace containing ash.

The Optimal Cloud Analysis (OCA) scheme nearing operational implementation at EUMETSAT is designed to retrieve water (liquid and ice) cloud properties; specifically optical depth (at a reference wavelength of 0.55 microns), particle size and altitude. The scheme shares a common history with the Oxford RAL Aerosol and Cloud (ORAC) scheme which is being developed in parallel at the University of Oxford and at the Rutherford Appleton Laboratory (RAL).

The basic algorithmic principle is the fitting of the observed SEVIRI measurements to values predicted by a fast radiative forward model (FM) by adjusting the cloud property values; all subject to error levels in the measurements and any prior information. This is accomplished by the optimal estimation (OE) approach [Rodgers] which seeks to minimise (via an iterative procedure) the cost function:

$$\phi^2 = (\underline{y} - F(\underline{x}))^t \mathbf{S}_y^{-1} (\underline{y} - F(\underline{x})) + (\underline{x} - \underline{a})^t \mathbf{S}_a^{-1} (\underline{x} - \underline{a})$$

Where

\underline{y} is a vector containing the measurements (channel radiances)

\underline{x} is the “state-vector”, containing the retrieved parameters (optical depth, effective radius, altitude and surface temperature)

$F(\underline{x})$ is the FM which predicts measurements for a given state.

\underline{a} is a prior estimate of the state expressing knowledge of the state in absence of the observations.

\mathbf{S}_a is a covariance matrix describing the uncertainty of \underline{a} . In this case we assume negligible prior constraint on all parameters except surface temperature (which is assumed to have an error of 1K over sea and 10K over land).

\mathbf{S}_y is a covariance matrix describing errors in the measurements (see section 5).

A fundamental assumption of the standard version of OCA is that cloud can be represented by a single geometrically thin layer. Scattering and absorption of radiative by the clouds is simulated offline and the results used in OCA through look-up tables (LUTs). Normally LUTs for liquid clouds (one type) and ice clouds (two types) are used. Cloud type can be identified in OCA by the “minimum cost method”: Retrieve cloud properties using LUTs for each cloud type in turn, and then select the result which gave the best fit to the observations (minimum value of the cost function). For water-cloud a more efficient approach (which should give the same result if the measurements are unambiguous) is to change the assumed cloud type during the iterative retrieval as generally (although not always) the radiance space occupied by liquid water clouds is separated from that occupied by ice clouds; the cloud particle size parameter is used to determine the phase.

Prior to this study, LUTs for volcanic ash were produced at RAL, using ash optical properties produced by the University of Oxford (Refractive indices were derived by Dan Peters¹ and Mie calculations based on these were performed by Elisa Carboni). These ash LUTs were applied to some test scenes from AATSR and MSG-SEVIRI, using an experimental version of the OCA/ORAC scheme that had been developed in the “Cloud-model” (CM) study [Siddans 2010]. These results showed some promise, so the current study was commissioned to further investigate the potential of OCA for identifying and retrieving properties of volcanic ash.

3 Usefulness of individual SEVIRI channels for ash detection and retrieval

The ability to distinguish ash from water cloud is based on the distinct spectral optical properties of ash, in particular its characteristic spectral refractive index. Figure 1 compares the Oxford ash refractive index used in this study with other ash models (Adesite-Pollack, Volz) and those of other potentially relevant materials including liquid water and ice. The starting point for these schemes [Prata 1989, Pavolonis 2009, CMSAF, Lean] is to apply a threshold to the difference between observed radiances at 11 and 12 microns. The gradient in the imaginary part of the ash refractive index (see figure 1) across the 10-12 micron range often leads to higher observed brightness temperatures (BTs) in the 12 micron channel than the 11 micron channel when ash is present (see figures 2 and 3). Under most other “normal” situations the opposite is the case (the refractive index of water has the opposite tendency and there is also more water vapour absorption at 12 microns). However there is no simple threshold value which can be applied to the 11-12 micron difference to unambiguously identify ash and so schemes are refined by using other channels or contextual information to robustly detect ash, avoiding false detections. E.g. ash is relatively highly reflective compared to liquid cloud at 3.9 microns, so during the day, the 3.9 micron channel can be useful for refining ash detection [Pavolonis 2006].

Other thermal IR channels can provide additional information with which to attempt to recover independent information on ash size, amount and layer height. In particular channels with significant trace-gas absorption (6.2, 7.3 and 13 microns) provide distinct information on height and the additional window channel at 8.7 micron channel provides further sampling of the spectral optical properties of ash which can potentially be used to infer ash particle size (if the composition is assumed to be well modelled). In principle the

¹ Refer to <http://www.atm.ox.ac.uk/project/aerosol/spectra.html>

9.7 micron channel could provide further information on size / composition if the strong effects of ozone absorption can be well modelled based on prior information (which is a realistic possibility but has not yet been fully explored).

As for water-cloud, the solar channels (0.6, 0.8, 1.6 microns) provide information on ash amount and size, however by themselves they do not enable ash to be clearly distinguished from water cloud (the IR channels are more specific in this respect). Shorter wave channels (even having 0.55 in addition to 0.67 as is the case for AATSR, but especially “deep blue” channels such as 0.4 microns) would provide a distinct ash signature as ash absorbs at those wavelengths.

Figures 2 and 3 show some example radiative transfer calculations (performed with the OCA fast FM) which illustrate some of the points above. In particular the distinct 11-12 micron BT difference can be observed. Note that at high optical depth and / or effective radius this difference reduces to zero (as the ash becomes a black body in both channels).

It is important to note that in general no channel is uniquely sensitive to a given retrieved parameter (all parameters effect all channels to a greater or lesser extent). The sensitivity of channels depends on the background atmospheric conditions and the retrieved parameters themselves. One key potential benefit of OCA is that it fits channels simultaneously, properly modelling the background state, and thereby optimally resolving the otherwise ambiguous dependencies of observations in each channel on a given state parameter. Because of this, it may be that OCA can identify ash more skilfully than a simple threshold-based scheme, since the need to carefully set criteria applicable to all observing conditions is avoided – the cloud type which most consistently matches observations (and prior information) should be selected.

The following issues with regard to modelling specific channel radiances in the context of ash retrievals are noted:

- In current OCA water cloud retrievals it is often difficult to obtain a consistent fit in the 1.6 and 3.9 micron channel simultaneously. Because of this, the 3.9 micron channel is usually only fitted passively in cloud retrievals (i.e. measurement errors is set so large that the channel effectively not used by the retrieval). The causes of this fit discrepancy are not fully understood (see [Siddans 2011]) but may also affect the use of this channel for ash detection / retrieval. For this reason we do not generally use the 3.9 micron channel in the retrievals performed for this study.
- The 6.2 and 7.3 micron channels are particularly sensitive to correctly modelling water vapour. OCA currently uses ECMWF data to define the water vapour profile. [Siddans 2010] estimated forward model errors due to errors in the ECMWF profiles (after interpolation to the SEVIRI observation time and spatial resolution) to be up to a few Kelvin (in BT). If such errors are assumed in retrievals, the potential benefit of the channels is greatly reduced compared to the ideal case in which only measurement noise need be considered. In the current OCA scheme at Eumetsat however, retrievals have been shown to benefit from using the water vapour channels with forward model errors of 0.4K.
- The 7.3 and 8.7 micron channels are sensitive to SO₂ which is often produced by volcanic eruptions and is often (though not always) co-located with ash in volcanic plumes. Figure 4 shows some radiative transfer simulations of the effect of varying column abundance of SO₂ on these channels. These simulations have

been performed using the RTTOV9 model [Matricardi], using coefficients which allow SO₂ to be varied. These were produced at RAL using the method of [Siddans 2011]. It is noted that the impact on these channels is less than 0.5K if the column of SO₂ is less than 10DU (for typical observing conditions). GOME-2, OMI and IASI (which are more sensitive to SO₂) report generally smaller SO₂ amounts than 10DU for the Icelandic eruption, so for this study we proceed without further considering the impact of SO₂ on the SEVIRI ash retrieval. This would not be appropriate for other volcanic eruptions which may produce much larger amounts of SO₂. In those cases, however, it is noted that joint retrieval of SO₂ and ash may well be possible with OCA.

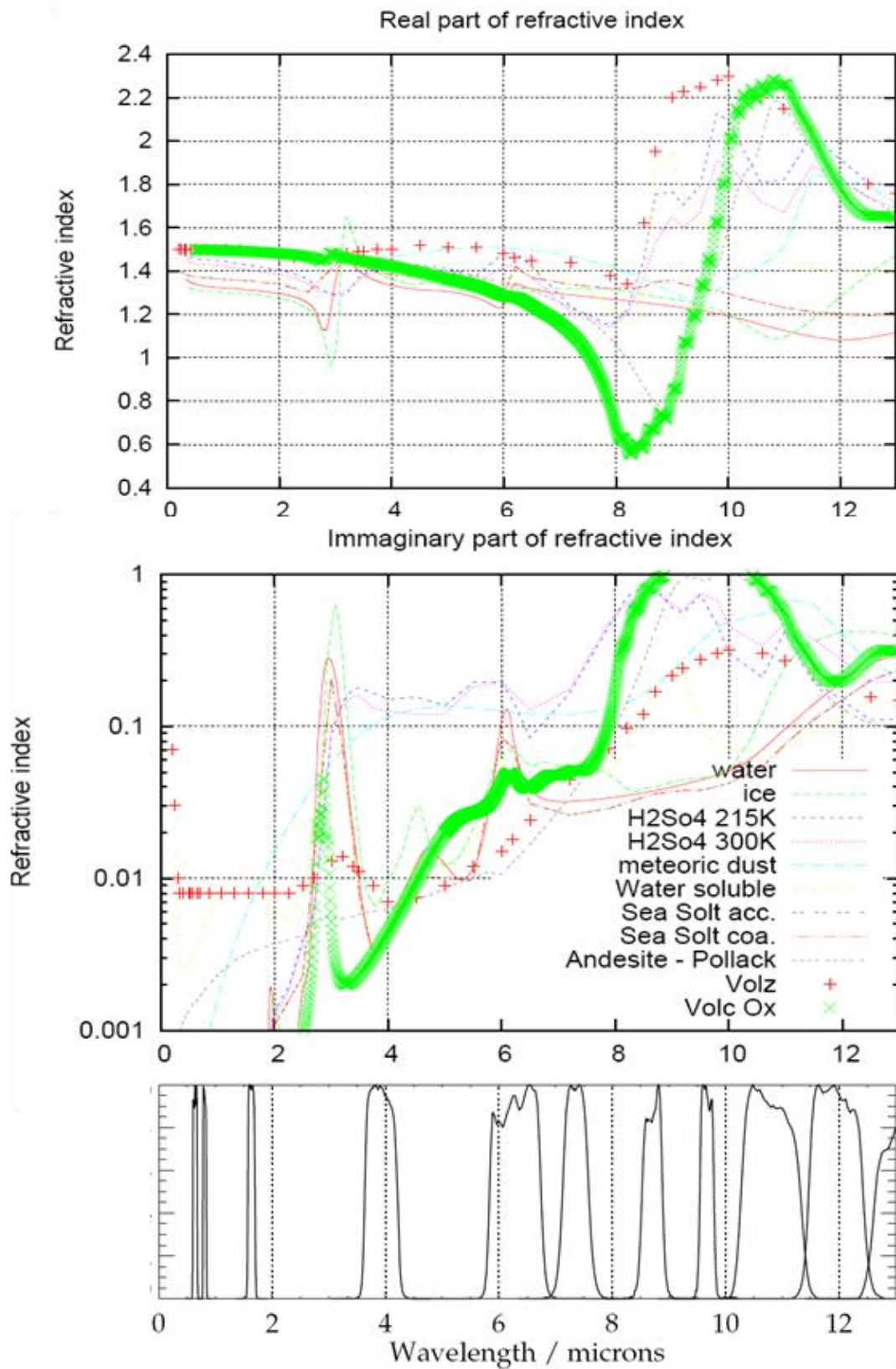
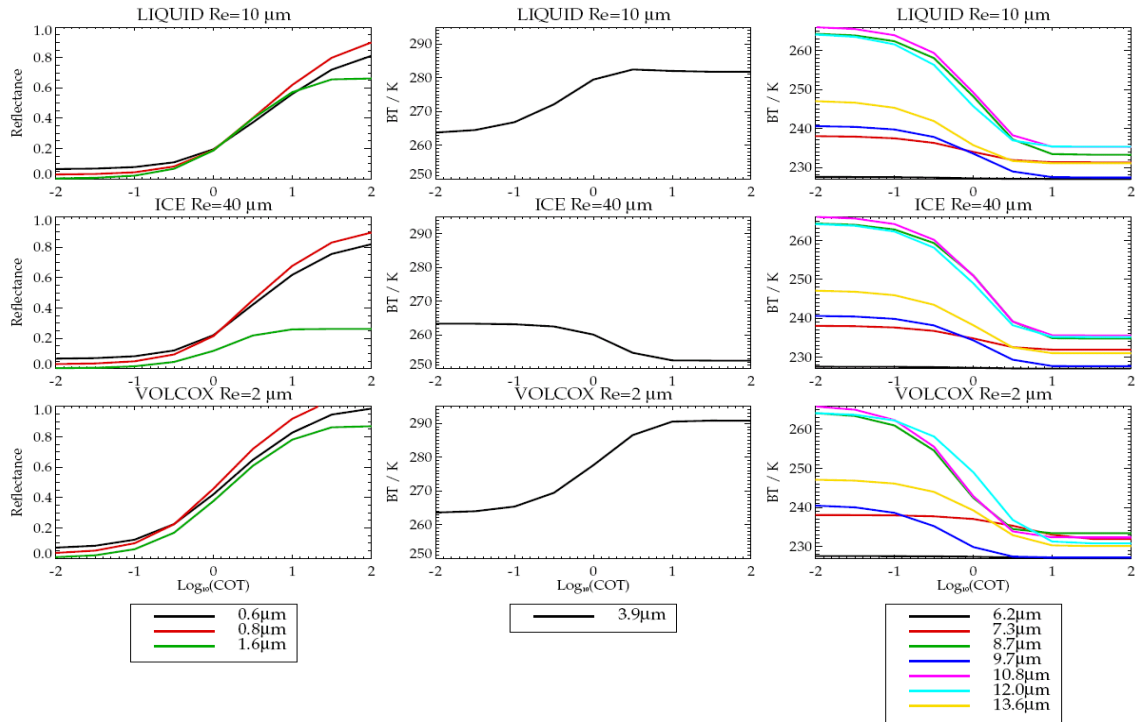


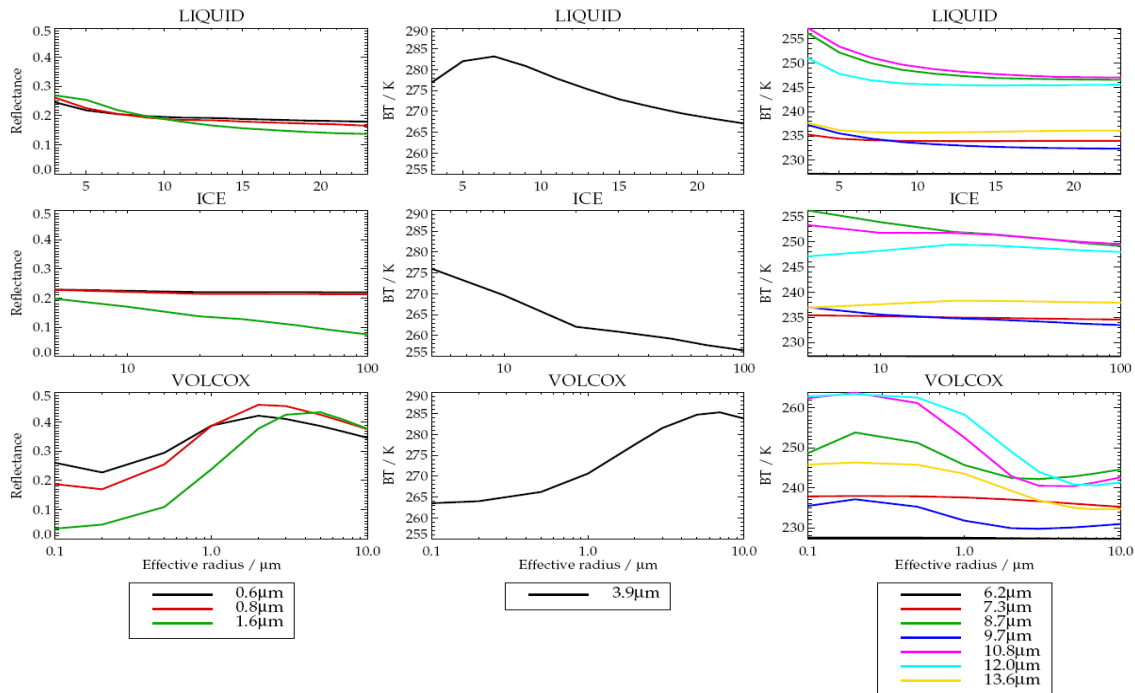
Figure 1: Real (top) and Imaginary (centre) refractive index of various compounds including water cloud and volcanic ash. Bottom panel shows the SEVIRI spectra response functions (arbitrary y-axis). Green “x” symbols show the volcanic ash properties measured by Dan Peters, used throughout this work. Top panels were prepared by Elisa Carboni of Oxford.



09:53 09/05/11.

LZA/SZA/Rel.azimuth: 60/60/160 deg.; Cloud-top pressure: 422 hPa.

Figure 2: Simulated SEVIRI measurements in each channel for varying cloud type (top-bottom) and cloud optical thickness (COT). Panels from left to right show channels grouped by spectra range (visible/near-infra-red, 3.9 micron channel, thermal infra-red). The assumed effective radius for each type is indicated above each panel.



09:53 09/05/11.

COT: 1; LZA/SZA/Rel.azimuth: 60/60/160 deg.; Cloud-top pressure: 422 hPa.

Figure 3: Simulated SEVIRI measurements in each channel for varying cloud type (top-bottom) and cloud effective radius. Panels from left to right show channels grouped by spectra range (visible/near-infra-red, 3.9 micron channel, thermal infra-red). All results are for a cloud optical thickness (at 0.55 microns) of 1.

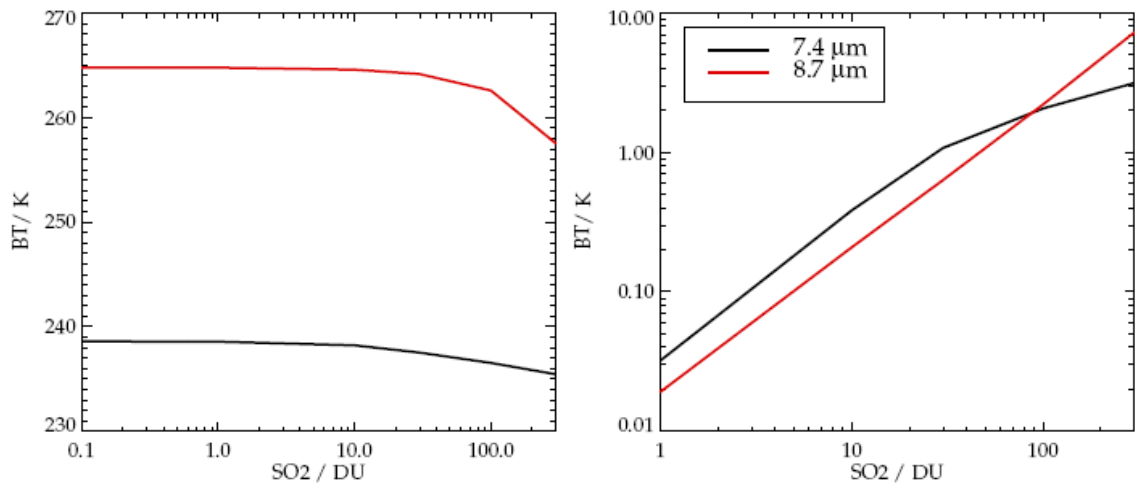


Figure 4: Left hand panel shows simulated radiances in the 7.4 and 8.7 μm channel for varying column amounts of SO₂. View zenith angle is assumed to be 60°. SO₂ is assumed to be in an infinitesimal layer at an altitude of 6km. Right hand panel shows the difference between the radiance when SO₂ is included and a simulation with no SO₂.

4 Data-set analysed

In this study we have applied the CM-study version of the OCA scheme to a sub-set of the SEVIRI data spanning the Eyjafjallajokull eruption from 6-18 May 2010.

This period is chosen in preference to the earlier episode in April as (a) the ash plume developed mainly over ocean and (b) there are many more suitable coincidences with CALIPSO which can be used to validate the retrievals. Land is avoided not because it would necessarily present a fundamental problem for the scheme, but because the version of OCA used here is not fully optimised for use over land (the CM-study focussed on retrievals over sea) and there was insufficient resource in this study to develop the scheme and/or establish confidence in its performance over land.

From 6-10 May, one scene per hour has been analysed over a large region of the observed Earth disk.

From 6-18 May, sub-scenes have been processed which co-locate with all orbits of CALIPSO identified as sampling through the ash plume [Prata, pri.comm, see section 11].

We focus mainly on detection and retrieval during day-time. Again this is largely because the scheme is not optimised for night-time retrievals. However, as described below, a two-layer infra-red only scheme has been developed for this study and this has been applied to both day and night observations co-located with CALIPSO. As discussed above, the infra-red channels contain sufficient information to unambiguously resolve ash amount, size and height, so one would expect night-time retrievals of ash to perform well.

5 Retrieval scheme configuration

Most retrievals performed here have the following characteristics

- All channels are fitted except 3.9 and 9.7 microns.
- Measurement errors are shown in table 1. Two options for the measurement errors in the water vapour channels are tested: (1) with errors as currently used in OCA at Eumetsat (2) with errors increased to reflect a more conservative estimate of the likely forward model (FM) error caused by errors in the assumed water vapour profile (which in this case comes from interpolating 1.25° resolutions, 6 hourly sampled ECMWF data to the location and time of each SEVIRI observation).

Standard single layer retrievals have been performed using the “minimum cost” method to identify the “best” type (liquid water, ice, ash) for each SEVIRI observation. The minimum cost method is slightly adapted to only report ash if it has a cost 10% smaller than the cost of water cloud. I.e. ash will not be selected if its cost is the same as the other cloud types.

It is clear that only very few scenes contain only volcanic ash (most contain ash over thick liquid water cloud). In these circumstances the single-layer OCA retrieval is often inappropriate, so we have implemented for this study a two-layer retrieval scheme.

Following an approach recently implemented at Eumetsat, this scheme uses only the IR channels and retrieves the following:

- Optical thickness, effective radius and height of the upper layer which is assumed to consist of either ice or ash.
- Altitude of an underlying liquid cloud, which is assumed to have a cloud optical thickness (COT) of 31 ($\log_{10}(\text{COT}) = 1.5$) – i.e. effectively an opaque layer.

In daytime we select the minimum-cost two-layer retrieval (ash or ice) for a scene if the minimum-cost single-layer retrieval has a normalised cost > 2 .

At night-time we do not have a (suitably optimised) single-layer retrieval, so we simply select the minimum cost two-layer retrieval result.

Channel (microns)	Noise	Co-registration / %	Homogeneity / %	Trace-gas variability
0.67	0.000274	2	0.75	
0.87	0.000385	2	0.75	
1.6	0.000904	1.5	1	
3.9	<i>0.25 K</i>	<i>0.15</i>	<i>0.5</i>	
6.2	0.05 K			0.4 or 3 K
7.3	0.06 K			0.4 or 2 K
8.7	0.15 K			
9.7	<i>0.11 K</i>			
10.8	0.21 K			
12.0	0.23 K			
13.4	0.35 K			

Table 1: Components of the measurement error assumed for each channel. Channels in italics are not used.

6 Ash Detection with OCA

Here we deal with the issue of determining when to apply the ash LUTs in OCA. Currently the choice between ice and liquid water LUTs is made during retrieval iteration. The choice to switch between LUTs is made based on simple tests on the retrieved state (in particular the effective radius) as it converges towards the solution. The same approach cannot obviously be simply generalised to extend OCA to deal with another particle type such as volcanic ash.

Possible solutions to this are (a) least cost method or (b) external flagging.

In (a) (the most expensive computationally) all possible target types are run (liquid, ice phase water, and ash) and the result giving the best radiance fit (least 'cost') provides the scene type and therefore the ash 'detection'. A cheaper hybrid of this would be to run two options, the current OCA water-phase selecting version and the ash model and then select the lower cost result. As the cost of the standard cloud-only OCA is considered to be high, neither solution is likely to be implementable. (b), external flagging by some radiance signature, if robust, would be best from a computational point of view.

A further option is to apply the 'least cost' method only following a high cost result in the standard run, although, because multi-layer clouds cause high cost and are frequent (~20-40% cases) this may also be expensive given the comparative rarity of ash incidence. In a similar approach, external flagging might be applied only following high cost in the standard run; this might reduce false alarms from the flagging method.

To inform selection of an appropriate strategy, some retrieval results (based upon applying the minimum-cost method) are presented:

Figures 5-8 show some scenes around Iceland at 12:12UT on the 6-9th May. These figures show the following:

- Top left: Cloud optical thickness (COT)
- Top centre: Cloud effective radius (Re)
- Top right: The cloud top pressure, p, expressed approximately as altitude:
$$Z^* = 16 (3 - \log_{10}(p))$$

(At the latitudes of interest here this tends to underestimate geometric altitude by up to ~1km.)
- Centre left: The ash mass column density (calculated by integrating the assumed log-normal size distribution and assuming a density for the ash material of 2.6 g/cm³ [Pavolonis 2009].
- Centre: Visible / near-ir false colour image.
- Bottom left: The selected cloud type is here indicated by the basic colour (grey, blue, red). Darker shades indicate where the cost function (normalised by the number of fitted channels) is greater than 2 (i.e. the observations are significantly different from the fitted result).
- Bottom centre: The 11-12 micron BT difference (where less than -0.1 K)
- Bottom right: False colour composite based on the 8.7, 11 and 12 micron channels which typically shows ash as shades of orange, pink or peach.

The legend provides a few statistics based on the presented data:

1. Min.cost = ash: The number of scenes where ash is selected by OCA, applying the minimum cost method.
2. 11-12µm < - 0.1K: The number of scenes where the 11-12 BT difference is smaller than -0.1K.
3. Operational mask: The number of scenes which would be flagged as ash applying the over sea scheme from [NWC-SAF]
4. The number of cases where (2) applies and the minimum cost of either phase of water cloud is larger than 2.
5. The number of cases where both (1) and (2) apply, i.e. the BT difference is less than -0.1 K and the scene is identified by OCA as being ash.
6. The number of cases where (1) and (2) apply and the cost of either phase of water cloud is larger than 2.

Figures 9-13 show the bottom 3 panels of figures 5-8 for four times of day from 08:12 on 6 May to 15:12 on the 10th. These figures show results over a much larger area.

The following points may be noted:

- Ash often seems to be correctly detected (judging by the 11-12 difference and the interpretation of the false colour images).

- Outside of plume, false detections either at low optical depth (<0.2), or “noise” mainly around cloud edges. The latter points could easily be excluded by simple filtering (as described in [Pavolonis 2009]).
- The 11-12 BT difference is very often less than -0.1K outside the ash plume. In particular in the scene analysed here it is very often negative over the pervasive liquid cloud which lies under a pronounced boundary layer temperature inversion (diagnosed by ECMWF). Under these circumstances water vapour emission above the cloud (where the temperature is higher) leads to a “false ash” signal. These false detections are almost always avoided by OCA as it can reproduce the negative 11-12 BT difference with a liquid cloud, given the correct temperature and humidity profiles for the relevant locations.
- On the other hand, OCA sometimes identifies what seems to be ash where the 11-12 micron difference is not negative (or at least larger than -0.1K). This is clearly seen near to the volcano, e.g. see figure 7, where the plume is thick and is sometimes associated with relative large effective radius. The 8.7/11/12 false colour image shows these cases as a dark red/purple shade associated with the bright-red plume easily detected by the 11-12 BT difference. Animations show this apparent plume moving somewhat differently to the bright plume indicating there may be some difference in altitude (the dark plume perhaps appearing to be higher). Possibly there may be ice present in the darker plume, affecting the 11-12 micron difference, however one should note that OCA can reproduce the observed positive 11-12 difference with its single-layer ash model (see also figure 23 below and associated discussion). One can exclude the possibility that the darker plume is SO_2 as this would have no impact on the 11-12 BT difference.
- The ability to detect ash where it is thick, close to the source is extremely important for early warning applications, so the potential for OCA to identify such cases which may be missed by a simple 11-12 micron flag is important.
- Largely because of the additional ash detections (but also partly because of OCA falsely detecting ash away from the main plume), statistic (5) is often significantly smaller (10s%) than (1). i.e. if one only attempted an OCA-ash retrieval when the 11-12 difference was less than -0.1K , then a large number of ash scenes would be missed.
- However, statistic (6) is not much lower than statistic (5), indicating that very few scenes ultimately identified as ash have a low cost for water-cloud.
- We have also calculated the NWC-SAF flag, however this is very conservative (only identifying very clear ash, carefully avoiding false detections). Statistic (3) shows that OCA identifies far more ash (though no doubt has also more false detections).
- OCA sometimes selects liquid cloud despite a large negative 11-12 BT difference. This occurs when relatively thin ash appears over thick liquid cloud. Generally speaking, in these situations OCA reports liquid with a high cost, indicating that liquid is not perfectly consistent with the observations. This shortcoming of the minimum-cost approach (switching from one class to another as the latter begins to dominate) is a consequence of the scheme reporting the type most consistent with observations, rather than attempting to identify when ash is present to a minor extent in mixed scenes. It might be possible to address this by developing a more continuous “ash probability”, using the relative cost for ash vs. that obtained for water cloud, though we have not pursued this idea further here.
- One should of course be cautious interpreting the ash retrieved amounts when the scene is mixed. In particular the optical thickness is likely to represent the total optical thickness of ash and underlying liquid cloud (so the derived mass is likely to be a significant overestimate).

- It is noted that the spectral signature of desert dust might be confused with ash. The location analysed means this issue is largely avoided here, but should be considered in future.

Based on this analysis we conclude as follows regarding the approach to apply OCA for ash operationally:

- OCA should first be applied in the standard way.
- Scenes which have a high cost for water-cloud should be considered for ash retrieval. However high cost occurs too often (30-40% of scenes due to multi-layer or mixed phase cloud) to consider applying the ash scheme in all these cases.
- A flag is therefore needed to identify which of these scenes to consider further
- Standard ash flags of often conservative (try to avoid false positives) and are therefore now suitable for this purpose. For OCA we require a flag which indicates the possible presence of ash (avoiding false negatives).
- The simple 11-12 BT difference $<0.1K$ test used here is not adequate as this will sometimes miss ash in some important cases (near to the volcano, at an early stage of the eruption).
- If this mask had been good enough, it would result in of order 5% of scenes being processed with the ash flag in the large region analysed here (i.e. a small increase in computational cost).
- It is expected that a more suitable mask could be defined, e.g. making use of 3.9 and 8.7 micron radiances as in [Pavolonis 2009, 2006]. We would not expect such a mask to lead to more scenes being processed than estimated for the simple 11-12 flag (indeed it may be less as some false positives might be avoided by more specific test).

It should therefore be possible to apply OCA to derive ash information without increasing its computational cost by more than 5% (and even this figure may be an overestimate). However further work is required to define a suitable “possible ash” flag.

7 Example retrievals along CALISPO orbits

Figures 14a-18c show day-time retrievals co-incident with CALISPO overpasses which sample the ash plume. In each case three different retrievals are shown:

- Figures (a) show single layer results.
- Figures (b) show results from the two layer scheme with 0.4K measurement errors on the 6.2 and 7.3 (water vapour) channels. Two layer results are only shown if the single-layer scheme results in normalised cost > 2 (otherwise the single-layer result from the corresponding figure (a) is shown. When the two-layer result is shown, the reported quantities relate to the upper cloud layer.
- Figures (c) show results as (b) except that in this case errors on the 6.2 and 7.3 micron channels are relaxed to 3 and 2K respectively.

In all cases, only results for the type selected by the minimum cost method are shown.

In each figure, the following quantities are shown (from top to bottom):

- The CALISPO measured back-scatter as a function of latitude (along the orbit-track) and altitude. On top of this is plotted the OCA retrieved cloud height. Letters are used to indicate the retrieved height, with different letters indicating different ranges of solution cost function value (indicated by the caption on the right).

Lower case letters indicate the retrieval did not perfectly converge. Colours indicate the type selected: Red is ash, black is liquid cloud and blue is ice cloud. A faint solid line shows an estimate of the cloud-top observed by CALIPSO. This altitude is used to identify the closest SEVIRI observation to each CALIPSO observation, accounting for parallax. Note that here the OCA values are geometric altitude (not Z^* plotted previously), derived from the retrieved cloud pressure using ECMWF data. Error bars show the estimated error on the OCA altitude, provided the error is large enough to extend beyond the letter.

All figures below are along- vs. across CALIPSO track images. The CALIPSO track runs from left to right along the centre of these panels. The swath shown (plotted along the y-dimension) is 100km wide. In all panels vertical lines show every integer degree of latitude (to guide the eye comparing panels).

- 0.6, 0.8, 1.6 micron measured false colour image.
- 0.6, 0.8, 1.6 micron false colour image as simulated by the OCA FM for the solution state. Note that in the two layer case this will show thick white cloud where the two layer model is applied, since the latter assumes thick liquid cloud to be below the upper layer (and only infra-red channels are fitted).
- 8.7, 11, 12 micron measured false colour. Panels on the left and right show respectively:
 - The mean (ECMWF) temperature profile along the section shown.
 - The location of the orbit section as a magenta line on a map.
- 8.7, 11, 12 micron image as simulated by the OCA FM for the solution state.
- The cloud-type identified by the minimum cost method.
- Flag indicating if the retrieval converged satisfactorily. Retrievals are judged to converge if (a) following the Marquardt Levenberg procedure [Rodgers 2000], absolute cost (not normalised by the number of measurements) reduces by < 1 from one iteration to the next (b) after this, a Newtonian iteration is attempted and this should also show a cost which reduced by < 1 . If both tests are satisfied then the flag is set to 1. If only (a) is satisfied then attempts are made to find a better minimum of the cost function by attempting various values for the Marquardt parameter. If these attempts are unsuccessful then the flag is set to -1. If the retrieval does not converge before reaching a defined maximum number of iterations then the flag would be set to 0, but this never occurs here.
- The solution cost function value (normalised by the number of channels fitted).
- Logarithm to the base 10 of the cloud optical thickness.
- Logarithm to the base 10 of the estimated error in the cloud optical thickness.
- Cloud (geometric) altitude in km.
- Estimated error in cloud altitude.
- Cloud effective radius in microns.
- Estimated error in the cloud effective radius.

Figure 14a shows results for an overpass on the 7 May. The single layer scheme clearly identifies the presence of ash around 48°N , but significantly underestimates its height, due to the presence of thick underlying liquid cloud. One can also see that the 8.7, 11, 12 micron false colour image is often well reproduced by the simulated radiances, but at the edges of the ash, the shades of peach abruptly change to green/brown. This reflects the abrupt change of identified cloud type from ash to liquid. This is also associated with rather high cost. A second (lower) ash layer around 52°N is not well detected. This layer is very difficult to detect as it lies just above the temperature inversion and has similar temperature to the liquid cloud below. The two layer retrieval (figure 14b) retrieves the 48°N ash layer height more accurately. Associated with this is a much better representation of the infra-red false colour image and identification of ash over a wider area (now the scheme can identify ash as a minor contributor to a mixed scene). The

estimated ash optical depth is much smaller than the single-layer result, while the effective radius is increased. The two-layer scheme detects more ash in the vicinity of 52°N, but this plume remains difficult to measure. Figure 14c shows two-layer results with a relaxed fit to the water vapour channels. Note that the error bars on the altitude of the 48°N plume increase (compared to 14b), and the height itself is not so well retrieved. However note also that the cost is now generally very low, so it is clear that there is difficulty fitting the water vapour channels to the 0.4K level, but in this case doing so seems to be beneficial for the retrieval results.

Figure 15a-c show results for a case in which CALIPSO samples the edge of an ash “plume” which is composed of several distinct vertical layers. The single layer scheme detects only a small proportion of the ash. Note also that the height of the ice cloud near 59°N is poorly retrieved. The two layer scheme does a much better job of identifying the thin ash (and thereby reproducing well the infra-red false colour), but it remains difficult to consistently match the CALIPSO height. In this case some of the differences will be due to co-location error. The two layer scheme retrieves the 59°N ice cloud height extremely well. Again tightly fitting the water vapour channels leads to increased cost but a better result. Structures in the cost field in 15b can be noticed with a scale-size of around 1 degree. Note that this corresponds to the resolution of the ECMWF data used, indicating that perhaps some water vapour errors are caused by using such relatively low resolution data (the ECMWF model resolution is around 16km but such high resolution data was not straightforward to obtain for this study).

Figures 16a-c show further thin ash layers which are better detected by the two layer scheme. Ash layer height is around 51°N is not perfectly retrieved. The spatial structure of the apparent height error in the top panel of figures 16b is of order 1° and so could be caused by water vapour interpolation errors. The ice cloud height beyond 60°N is very well retrieved by the two-layer scheme.

Figure 17a-c shows a case where ash occurs at low altitude, very close to apparent water cloud. Here the single layer scheme behaves quite well.

Figure 18a-c shows a case of very thin ash over liquid cloud, which is barely discernable in the infra-red false-colour image (though assumed to be present, based on the observed evolution of the plume in larger-scale false colour images, as a horizontal layer at around 5km altitude from 54-55.5°N). This plume is clearly at the limit of the ability of OCA to detect and retrieve useful information on ash.

Figures 19-24 show night-time results (hence the visible/near-ir false colour images are dark). In this study we have not optimised the single layer retrieval for night-time application (though this would of course be possible given time). We therefore simply show results from the two-layer infra-red scheme (which works equally well day or night). Note that the scheme by definition can only report ice or ash, assuming this to be over a liquid layer. If there is no ice or ash present then one would expect the scheme to report a negligible optical depth for the upper layer, however we have not screened the data in these plots to eliminate such negligible levels of ice or ash. This often leads to ice being false reported on the plots (though with very low optical depth and large estimated error in height). This could be avoided in future by first running an optimised single-layer night-time retrieval and only attempting the two layer scheme if a high cost is obtained. Despite this caveat, the results for ash are often very good.

Figure 23 shows an excellent coincidence of CALIPSO, sampling along the main, thick ash plume on this day. The plume has several layers from 2-6km and OCA performs quite well given this complex structure. Note that part of this plume does not produce a

negative 11-12 micron BT difference, though OCA detects it. Again this seen as a relatively dark red colour in the infra-red false colour image (which OCA reproduces very well).

Figure 24 shows the worst results found for ash height compared to CALIPSO. Given the behaviour of the cost, it could be that water vapour errors explain the high bias in the retrieved height.

Finally, figure 25 compares OCA results to those provided by M. Pavolonis [pri.comm.] based on applying GOES-R ABI scheme [Pavolonis, 2009] to SEVIRI. This scheme is based on first detecting ash using the 8.7,11 and 12 micron channels and then retrieving (with an OE approach) cloud effective temperature, effective emissivity and size. Height is inferred searching the analysed temperature profile for the retrieved effective temperature. Only results for the five cases were available. One case for 6 May was not analysed with OCA in this project. All other cases are shown. In most cases OCA provides results of comparable quality to that of the GOES-R scheme.

8 Summary and conclusions

The OCA scheme has been applied to analyse ash from the Eyjafjallajokull eruption in May 2010.

The “standard” single layer scheme is shown to be rather a powerful tool for detecting ash. It sees much more ash than NWCSAF flag and behaves better than a simple threshold on the 11-12 micron difference by (a) detecting ash which does not produce a negative BT difference, which is often the case when the ash is optically thick (b) eliminating many “false” detections that are produced by such a simple flag (because OCA correctly models the background radiative transfer). The capability to detect ash where it is missed by the 11-12 BT difference is potentially important for early detection of volcanic eruptions.

The main shortcoming of the scene identification from the single-layer OCA scheme is that, in mixed scenes (which are very common), it switches discontinuously from one type to another (depending on which component of the scene is dominant). Flags which seek to identify only the presence of ash may therefore perform better than OCA in this respect. More positively, it seems possible to identify mixed scenes by examining the retrieved cost function value at solution (so we know when mixed scenes may be causing problems in detection or retrieval). In mixed scenes one should of course use the OCA retrieved ash parameters with caution. When thin ash is present over thick liquid cloud, we expect single-layer OCA to over-estimate optical depth and under-estimate layer height (as clearly demonstrated by the CALIPSO comparison).

These problems can largely be overcome by the new two layer scheme which is capable representing and detecting ash over liquid cloud and returning properties for the ash layer alone, with appropriate estimated errors. Results for height compare well with CALIPSO and the GOES-R scheme. We have not assessed here how often the two-layer scheme falsely detects ash, however it is expected that one would need to carefully choose a minimum threshold for the retrieved ash optical depth (e.g. if this is two times larger than the associated estimated error) to avoid large numbers of false detections. It is also noted that it may be possible to translate the single-layer results into a more continuous ash probability, by examining the relative cost of ash compared to that of the other cloud types.

The two-layer scheme retrieves height with better precision and usually more accurately if the water vapour channels assuming a forward model error of 0.4K. This is sometimes an underestimate of the error in the assumed water vapour profiles (projected into measurement space) and seems to cause error in the retrieved heights in some cases. The water vapour errors may due problems in the ECMWF analysis itself or simply interpolation error (ECMWF fields were obtained at only 100km and 6 hourly sampling for this study, while the model is run at 16km resolution).

It is emphasised that the two-layer scheme used here was developed very quickly for this study. Further optimisation of the scheme is certainly possible (see further work suggestions below).

It has also been shown that it should be possible to implement the single-layer ash scheme operationally without increasing computational cost by more than 5%. This would be accomplished by only considering scenes which result in high water cloud cost and then only processing scenes flagged as potentially containing ash. Some further work is however required to define a suitable flag for this purpose (see suggestions for further work below).

9 Suggestions for further work

The following suggestions are made for further work, with the aim of developing a reliable consolidated ash product from SEVIRI based on OCA:

- OCA should be applied to other volcanic eruptions to demonstrate performance under a wider range of meteorological, surface and volcanic conditions e.g. Soufriere Hills, Karthala, Nyamagira, Etna.
- The analysis should be extended to cover (more completely than possible here) day and night-time observations over both land and sea. This would require some work to optimise the basic OCA scheme performance at night-time.
- Results from this extended analysis should be compared to those from other schemes applied to SEVIRI. In particular, alternative schemes considered for operational implementation at Eumetsat. Ash detection flags should be compared as well as retrieved quantities including mass.
- Develop a “possible ash” flag by using 3.9, 8.7, 11 and 12 micron channels to be used to identify scenes to which the ash version of OCA should be applied. This would be based on existing methods, such as that of [Pavolonis 2009] but with the emphasis shifted towards minimising false negatives. (The intention being that false positives would be eliminated later using the results from OCA.)
- For the single-layer scheme, as an alternative to identifying ash using the “minimum-cost” approach, consider deriving a continuous ash-probability using the OCA cost function values. An approach follows from Bayes’ theorem: The cost function values can be used as a measure of the probability of a given observation being consistent with the scene being ash, liquid or ice. Bayes’ theorem enables the probability of a given scene being ash to be calculated (also taking into account prior probabilities of each type).
- Develop ash detection criteria for the two layer scheme. It can be anticipated that if the minimum cost approach only was used to identify when ash is present then the two-layer scheme will produce a large number of false positives (although these will likely be accompanied by very low estimated ash amounts). If one wishes to unambiguously identify when ash is present, then criteria for what constitutes a significant amount of ash need to be defined.

- Implement and test the performance of an extended two-layer scheme which includes the solar channels.
- Test the sensitivity of the retrieval to assumed ash optical and microphysical properties. E.g. test sensitivity to varying the assumed ash refractive indices.
- The effect of SO₂ on ash retrievals should be further considered for cases in which large amounts of SO₂ are present. In particular, the capability of OCA to jointly retrieve SO₂ with ash should be tested. Note that the scheme employed in this study already has the capability to retrieve above-cloud SO₂ column but this was not found useful for Eyjafjallajokull.
- The benefit of using the 3.9 micron channel and the 9.7 micron channel should be assessed. Both should contribute significant useful information as discussed in section 3. In the latter case, sensitivity to realistic prior knowledge of the ozone profile (presumably taken from ECMWF analyses) would need to be assessed and traded against the potential benefit for ash (and water cloud).
- Options to improve the treatment of water vapour errors should be explored. In the first instance the impact of using full resolution ECMWF data should be tested. If remaining FM errors are still too large (as is likely to be the case), then options include (1) analysing large scale biases with respect to clear-sky observations; (2) more intelligently specifying the FM error as a function of either the channel radiance or the retrieved state (since these FM errors are likely to be larger when cloud is low and / or the radiance is high); (3) jointly retrieving water vapour.

Assuming Eumetsat intends to implement a fast scheme to retrieve ash mass, it is noted that the OCA could be used to characterise its performance. There could be two aspects to this characterisation (1) OCA could be applied to case studies and results compared to the fast scheme; (2) An error budget for the fast scheme could be developed by performing retrieval simulations in which the OCA 2-layer FM could be used to simulate radiances for known conditions which would input to the fast retrieval scheme.

Finally, it is also noted that the OCA scheme could be applied to derive ash from other Eumetsat instruments. E.g. application to IASI (perhaps jointly with AVHRR solar channels) would enable much more spectral information on ash to be exploited. Only a limited number of channels from the IASI spectral coverage would be needed, selected to minimise trace-gas interferences and computational cost. Work in this area is being carried out for water cloud at RAL through NCEO funded activities (however this does not extend to ash retrieval). Because of the additional spectral information, the IASI retrievals may be valuable in their own right as being more specific and sensitive to ash (one would certainly expect to be able to distinguish ash and desert dust and SO₂). However, analysing case studies with both SEVIRI and IASI could help diagnose the performance of the SEVIRI scheme. This would also pave the way for future retrievals from MTG which could benefit from the MTG-IR sounder, as well as the additional short-wave channels on the imager.

10 Supplementary Material

This report is provided at ftp://ftp.rsg.rl.ac.uk/cloud-model/volcanic_ash_study/dfr/

At that location are also

- 1) Two animations produced from figures like those shown in the report.
- 2) OCA format LUTs for ash as used in the study.

11 Collocating CALIPSO data

List of CALIPSO orbits which sample ash within the SEVIRI field of view, provide by F. Prata.

Date	SEVIRI Time	Calipso Time	Filename	
15.04.2010	04:00	04:01	CAL_LID_L1-ValStage1-V3-01.2010-04-15T03-52-34ZN.hdf	Maybe
15.04.2010	13:15	13:11	CAL_LID_L1-ValStage1-V3-01.2010-04-15T12-53-26ZD.hdf	
16.04.2010	01:15	01:21	CAL_LID_L1-ValStage1-V3-01.2010-04-16T01-18-07ZN.hdf	
16.04.2010	10:45	10:48	CAL_LID_L1-ValStage1-V3-01.2010-04-16T10-19-03ZD.hdf	
16.04.2010	12:30	12:37	CAL_LID_L1-ValStage1-V3-01.2010-04-16T11-57-54ZD.hdf	
17.04.2010	02:15	02:13	CAL_LID_L1-ValStage1-V3-01.2010-04-17T02-47-56ZD.hdf	
17.04.2010	03:45	03:50	CAL_LID_L1-ValStage1-V3-01.2010-04-17T03-40-21ZN.hdf	
17.04.2010	13:00	13:03	CAL_LID_L1-ValStage1-V3-01.2010-04-17T11-02-22ZD.hdf	
20.04.2010	04:15	04:16	CAL_LID_L1-ValStage1-V3-01.2010-04-20T04-11-30ZN.hdf	Maybe
20.04.2010	13:45	13:42	CAL_LID_L1-ValStage1-V3-01.2010-04-20T13-12-27ZD.hdf	Maybe
24.04.2010	04:00	03:56	CAL_LID_L1-ValStage1-V3-01.2010-04-24T03-47-03ZN.hdf	
06.05.2010	13:45	13:42	CAL_LID_L1-ValStage1-V3-01.2010-05-06T13-13-42ZD.hdf	
07.05.2010	03:15	03:18	CAL_LID_L1-ValStage1-V3-01.2010-05-07T03-17-14ZN.hdf	
07.05.2010	14:15	14:11	CAL_LID_L1-ValStage1-V3-01.2010-05-07T13-57-06ZD.hdf	
08.05.2010	04:00	04:05	CAL_LID_L1-ValStage1-V3-01.2010-05-08T04-00-33ZN.hdf	
08.05.2010	15:00	14:56	CAL_LID_L1-ValStage1-V3-01.2010-05-08T14-40-24ZD.hdf	
09.05.2010	04:45	04:43	CAL_LID_L1-ValStage1-V3-01.2010-05-09T04-43-56ZN.hdf	
09.05.2010	14:00	14:03	CAL_LID_L1-ValStage1-V3-01.2010-05-09T13-44-52ZD.hdf	
10.05.2010	04:00	03:56	CAL_LID_L1-ValStage1-V3-01.2010-05-10T03-48-24ZN.hdf	
10.05.2010	14:45	14:48	CAL_LID_L1-ValStage1-V3-01.2010-05-10T12-49-19ZD.hdf	
11.05.2010	13:45	13:52	CAL_LID_L1-ValStage1-V3-01.2010-05-11T13-32-37ZD.hdf	
12.05.2010	03:45	03:47	CAL_LID_L1-ValStage1-V3-01.2010-05-12T03-36-09ZN.hdf	
13.05.2010	13:45	13:45	CAL_LID_L1-ValStage1-V3-01.2010-05-13T13-20-24ZD.hdf	
14.05.2010	03:15	03:22	CAL_LID_L1-ValStage1-V3-01.2010-05-14T02-31-31ZD.hdf	
14.05.2010	12:45	12:48	CAL_LID_L1-ValStage1-V3-01.2010-05-14T12-24-52ZD.hdf	Maybe
14.05.2010	14:30	14:37	CAL_LID_L1-ValStage1-V3-01.2010-05-14T14-03-47ZD.hdf	
15.05.2010	02:45	02:47	CAL_LID_L1-ValStage1-V3-01.2010-05-15T02-28-24ZN.hdf	
15.05.2010	04:15	04:11	CAL_LID_L1-ValStage1-V3-01.2010-05-15T04-07-14ZN.hdf	
15.05.2010	13:45	13:40	CAL_LID_L1-ValStage1-V3-01.2010-05-15T13-08-10ZD.hdf	Maybe
16.05.2010	03:15	03:15	CAL_LID_L1-ValStage1-V3-01.2010-05-16T03-11-42ZN.hdf	
16.05.2010	04:45	04:48	CAL_LID_L1-ValStage1-V3-01.2010-05-16T03-58-12ZD.hdf	
16.05.2010	12:45	12:42	CAL_LID_L1-ValStage1-V3-01.2010-05-16T12-12-38ZD.hdf	
16.05.2010	14:00	14:07	CAL_LID_L1-ValStage1-V3-01.2010-05-16T13-51-28ZD.hdf	
17.05.2010	02:15	02:18	CAL_LID_L1-ValStage1-V3-01.2010-05-17T02-16-05ZN.hdf	
17.05.2010	04:00	04:01	CAL_LID_L1-ValStage1-V3-01.2010-05-17T03-55-00ZN.hdf	Maybe
17.05.2010	13:15	13:10	CAL_LID_L1-ValStage1-V3-01.2010-05-17T12-55-56ZD.hdf	
18.05.2010	03:15	03:10	CAL_LID_L1-ValStage1-V3-01.2010-05-18T02-59-28ZN.hdf	
18.05.2010	04:30	04:37	CAL_LID_L1-ValStage1-V3-01.2010-05-18T04-38-19ZN.hdf	Maybe
18.05.2010	12:35	12:37	CAL_LID_L1-ValStage1-V3-01.2010-05-18T12-00-25ZD.hdf	

12 References

Lean, K. Empirical methods for detecting atmospheric aerosol events from satellite measurements, Oxford University, EODG M.Phys report, http://www.atm.ox.ac.uk/group/eodg/mphys_reports/2009_Lean.pdf

NWC-SAF, Algorithm Theoretical Basis Document for "Cloud Products" (CMa-PGE01 v3.0, CT-PGE02 v2.0 & CTHH-PGE03 v2.1)

Matricardi, M.: Title The generation of RTTOV regression coefficients for IASI and AIRS using a new profile training set and a new line-by-line database Institution ECMWF Year of publication 2008

Pavolonis, M.J., Feltz, W.F., Heidinger, A.K., Gallina, G.M., A Daytime Complement to the Reverse Absorption Technique for Improved Automated Detection of Volcanic Ash,

JOURNAL OF ATMOSPHERIC AND OCEANIC TECHNOLOGY VOLUME 23, pp1422-1444.

Pavolonis, M, Sieglaff, J, GOES-R Advanced Baseline Imager (ABI) Algorithm Theoretical Basis Document For Volcanic Ash (Detection and Height) NOAA/NESDIS/STAR, Version 2.0, June 30, 2009

Prata, A.J. Observations of volcanic ash clouds in the 10-12 μ m window using AVHRR/2 data. *International Journal of Remote Sensing*, 10(4-5):751–761, 1989.

Rodgers, C.D., *Inverse Methods for Atmospheric Sounding : Theory and Practice* (Series on Atmospheric Oceanic and Planetary Physics), World Scientific Publishing Company (September 2000)

Siddans R, C. Poulsen, E. Carboni , Cloud Model for Operational Retrievals from MSG SEVIRI Final Report, Eumetsat Contract EUM/CO/07/4600000463/PDW, 2010

Siddans, R. Fast transmittance modelling of the MSG and MTG solar channels for cloud retrievals, Final Report EUMETSAT RFQ 10/202521

Thomas, H.E. and A. J. Prata, Sulphur dioxide as a volcanic ash proxy during the April–May 2010 eruption of Eyjafjallajokull Volcano, Iceland, *Atmos. Chem. Phys. Discuss.*, 11, 7757–7780, 2011

20100506121242.122_awat_ash_spi_zstar_v2p11

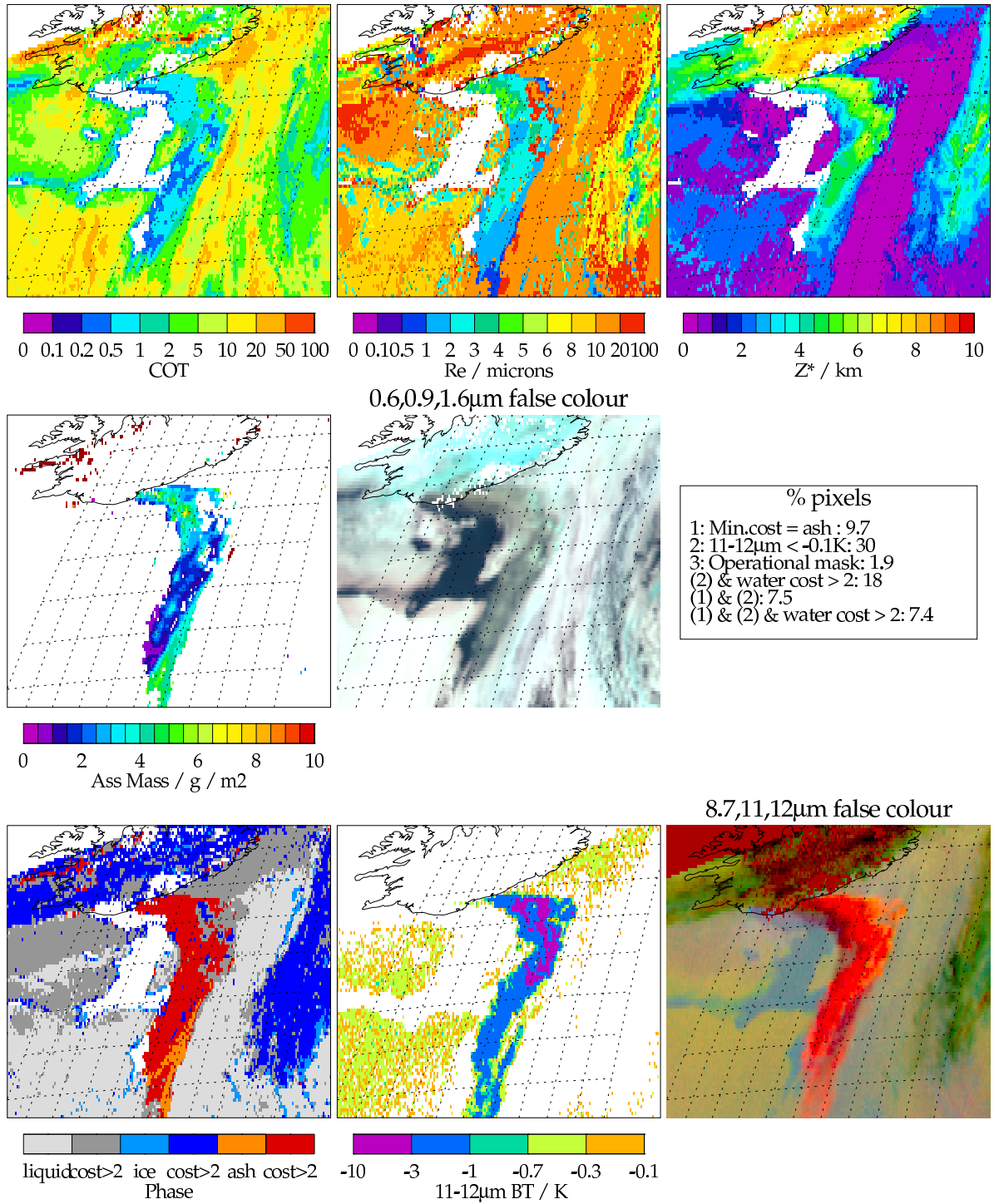


Figure 5: Retrieval output at 12:12 on UT on 6 May 2010.

20100507121241.877_awat_ash_spi_zstar_v2p11

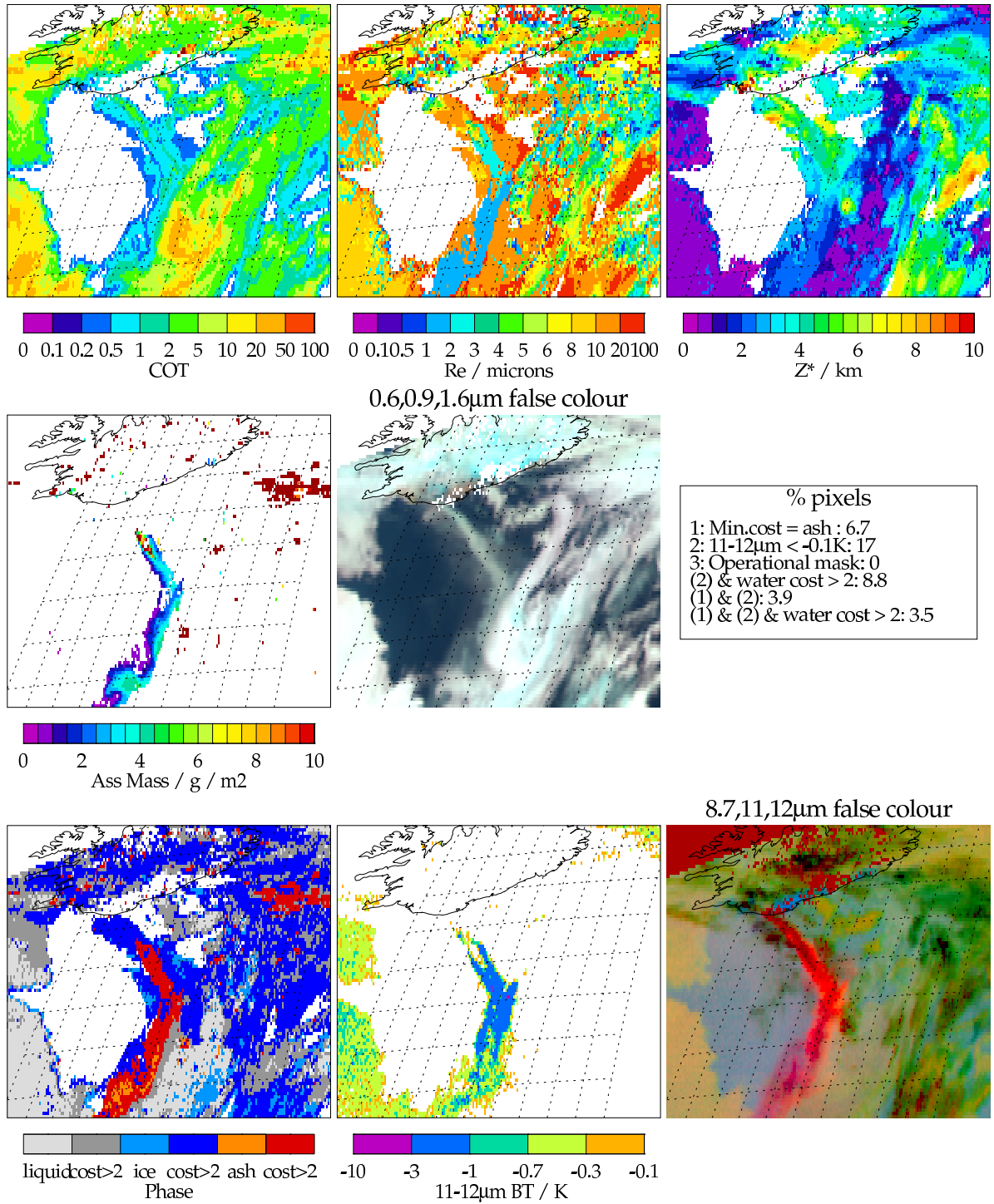


Figure 6: Retrieval output at 12:12 on UT on 7 May 2010.

20100508121241.463_awat_ash_spi_zstar_v2p11

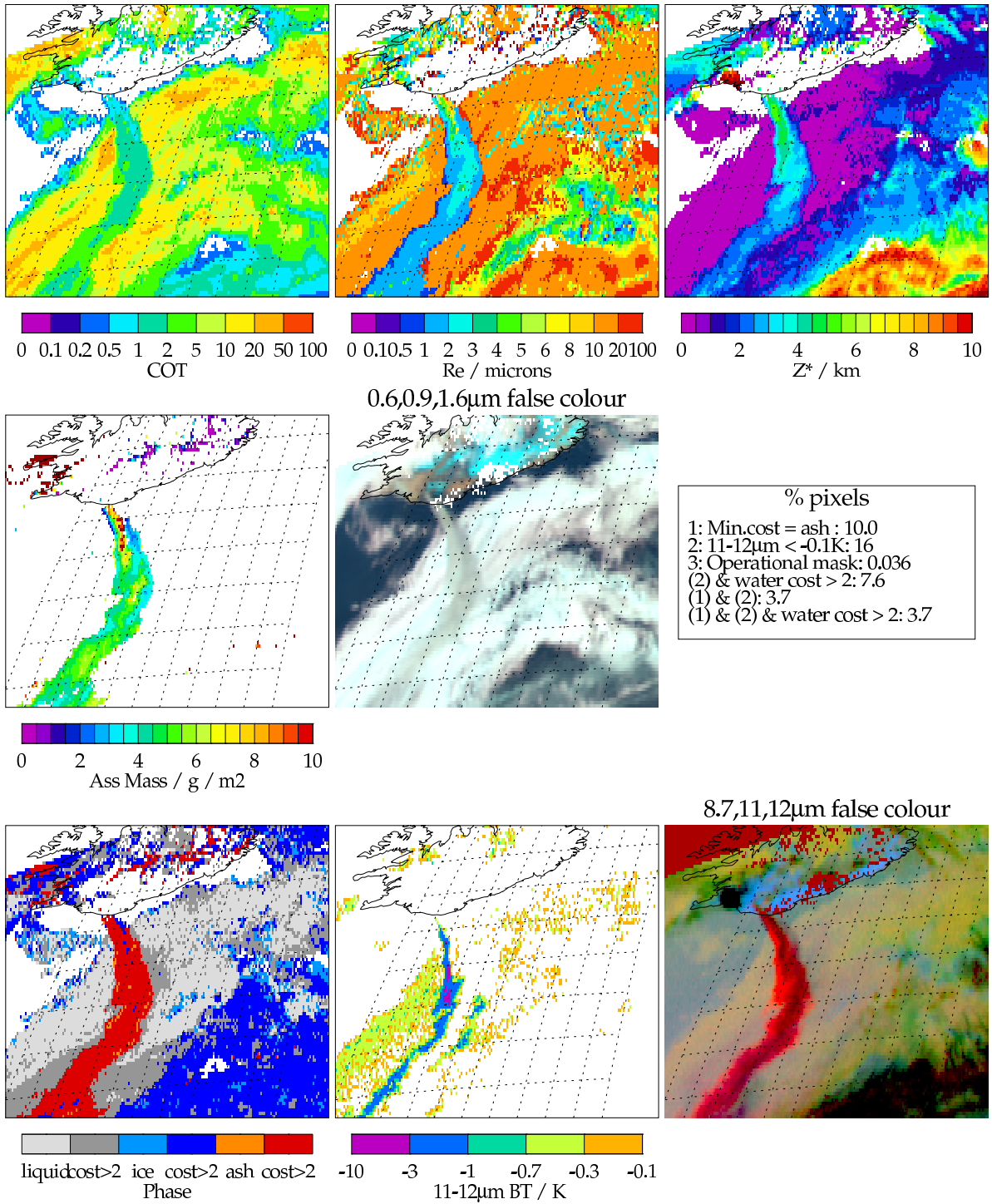


Figure 7: Retrieval output at 12:12 on UT on 8 May 2010.

20100509121241.448_awat_ash_spi_zstar_v2p11

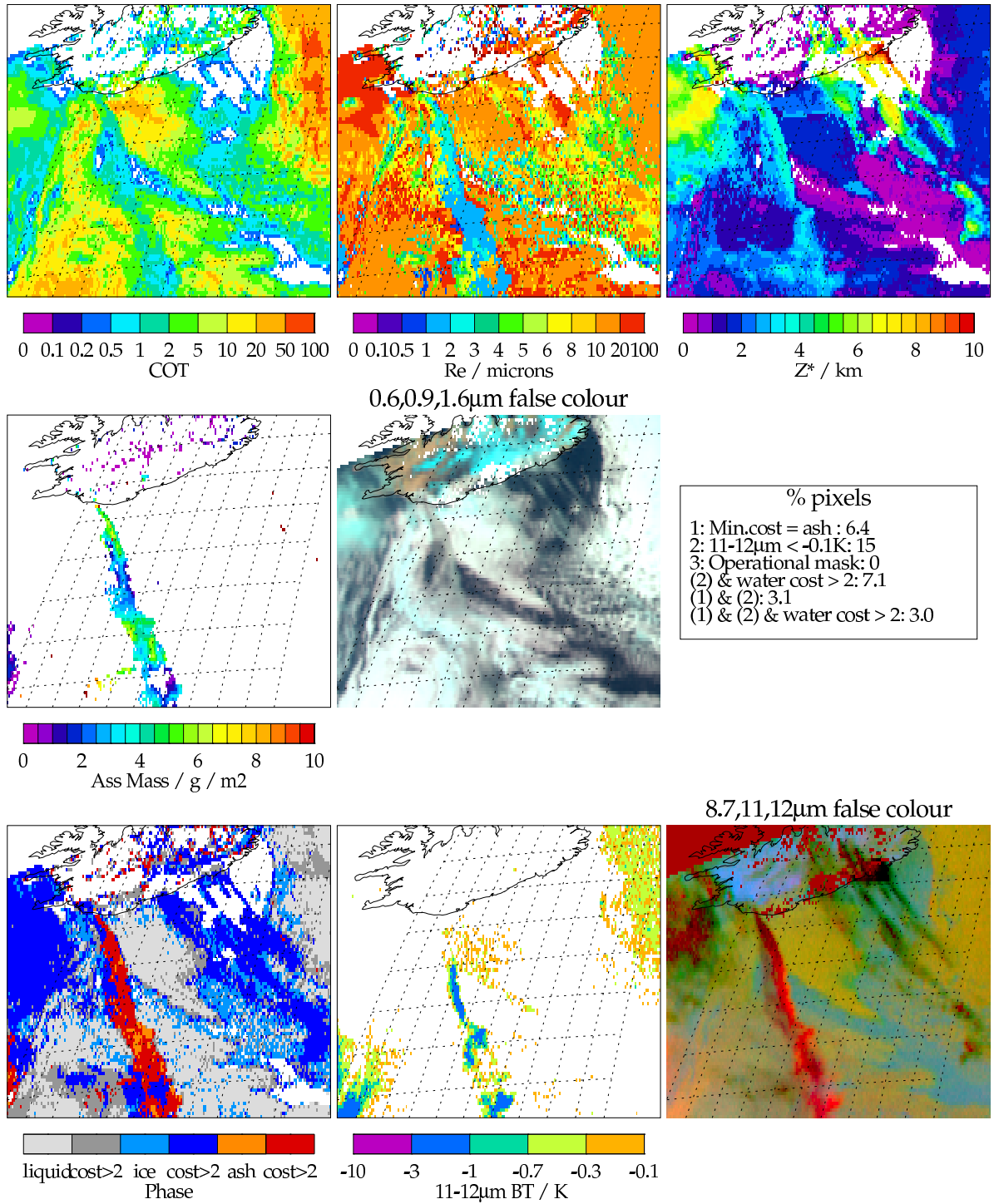


Figure 8: Retrieval output at 12:12 on UT on 9 May 2010.

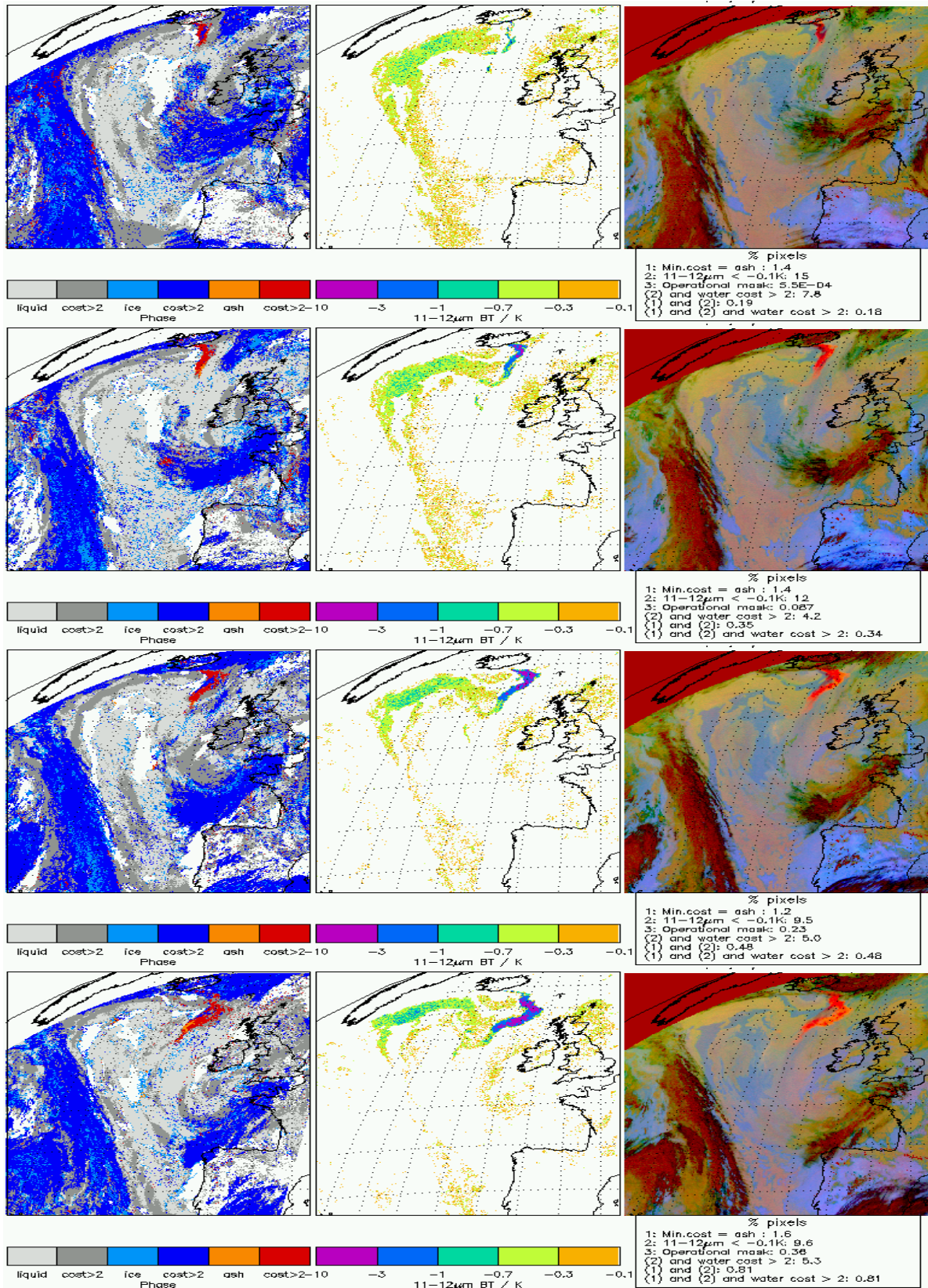


Figure 9: Cloud type, 11-12 μm brightness temperature difference and 8.7, 11, 12 μm false colour image for 9:12, 12:12, 15:12 and 18:12 UT on 6 May 2010.

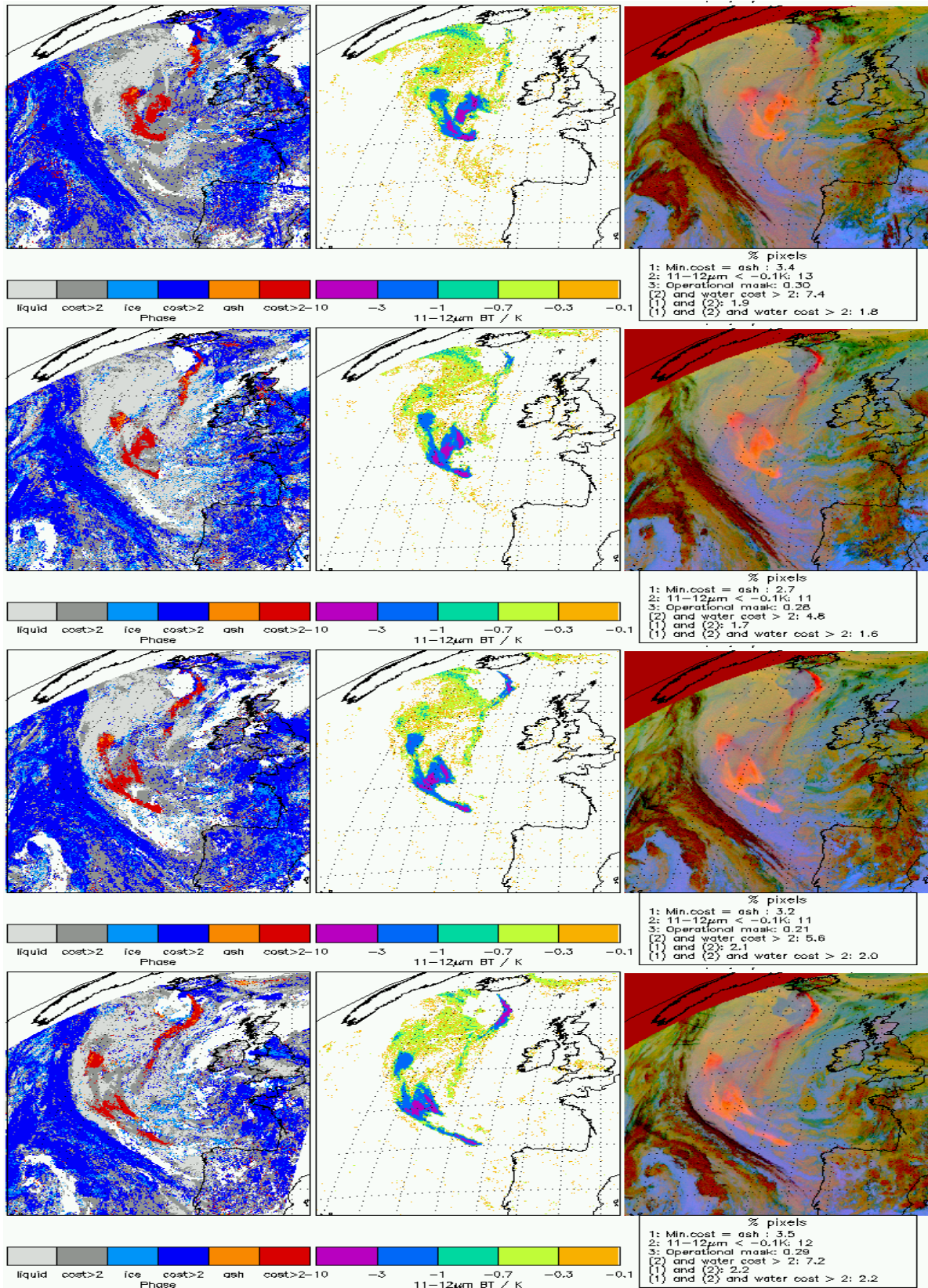


Figure 10: Cloud type, 11-12 μm brightness temperature difference and 8.7, 11, 12 μm false colour image for 9:12, 12:12, 15:12 and 18:12 UT on 7 May 2010.

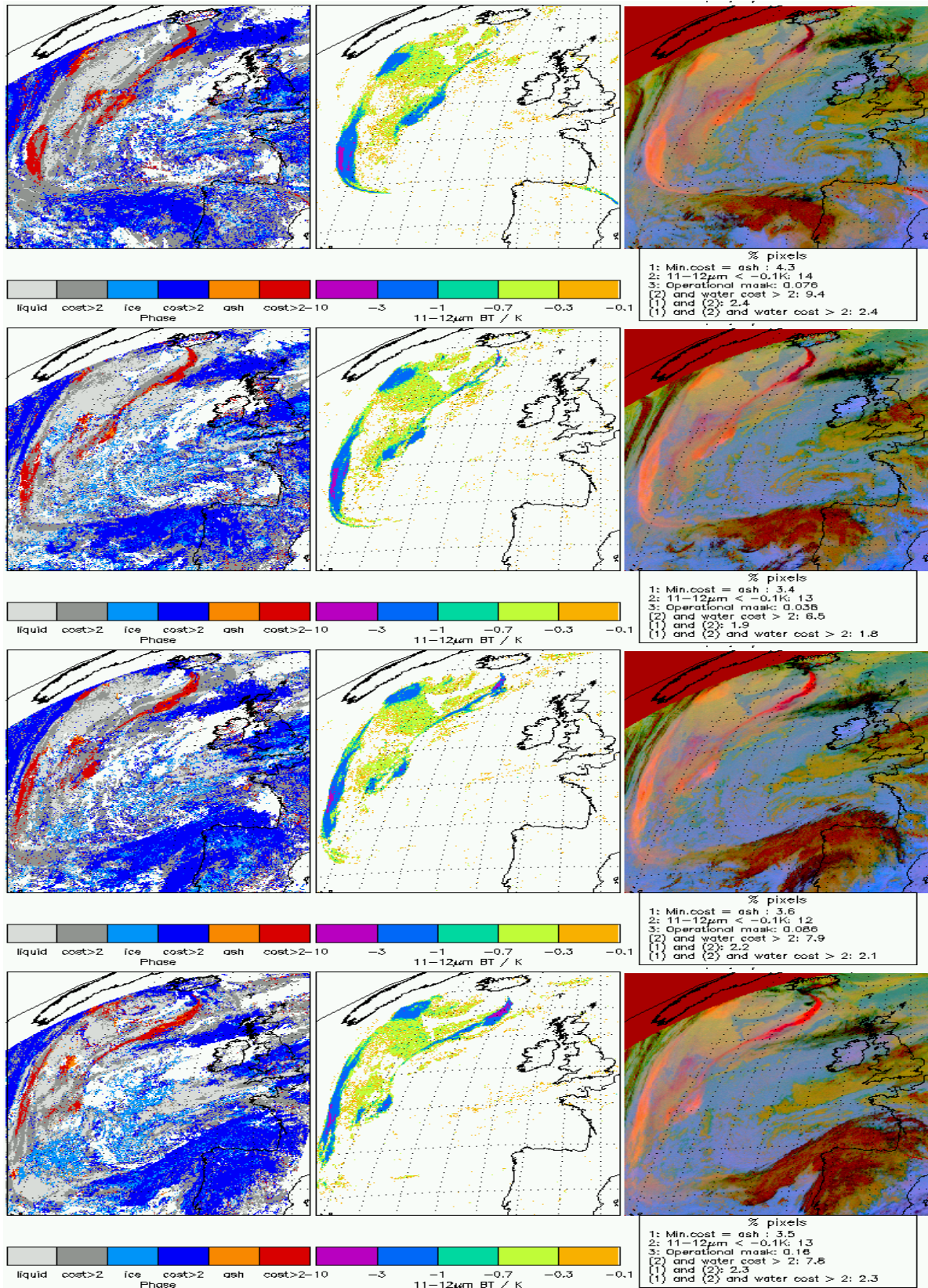


Figure 11: Cloud type, 11-12 μm brightness temperature difference and 8.7, 11, 12 μm false colour image for 9:12, 12:12, 15:12 and 18:12 UT on 8 May 2010.

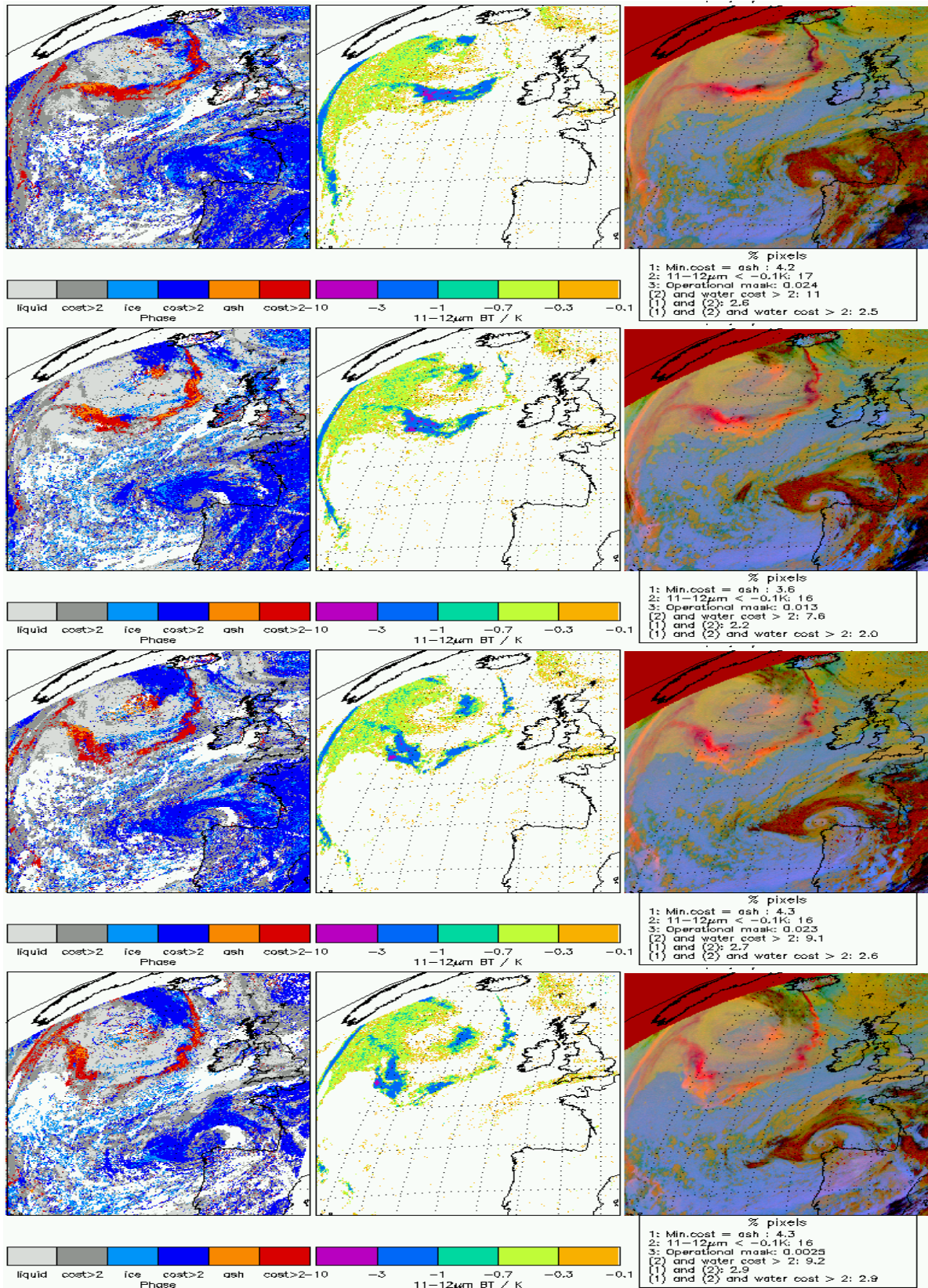


Figure 12: Cloud type, 11-12 μm brightness temperature difference and 8.7, 11, 12 μm false colour image for 9:12, 12:12, 15:12 and 18:12 UT on 9 May 2010.

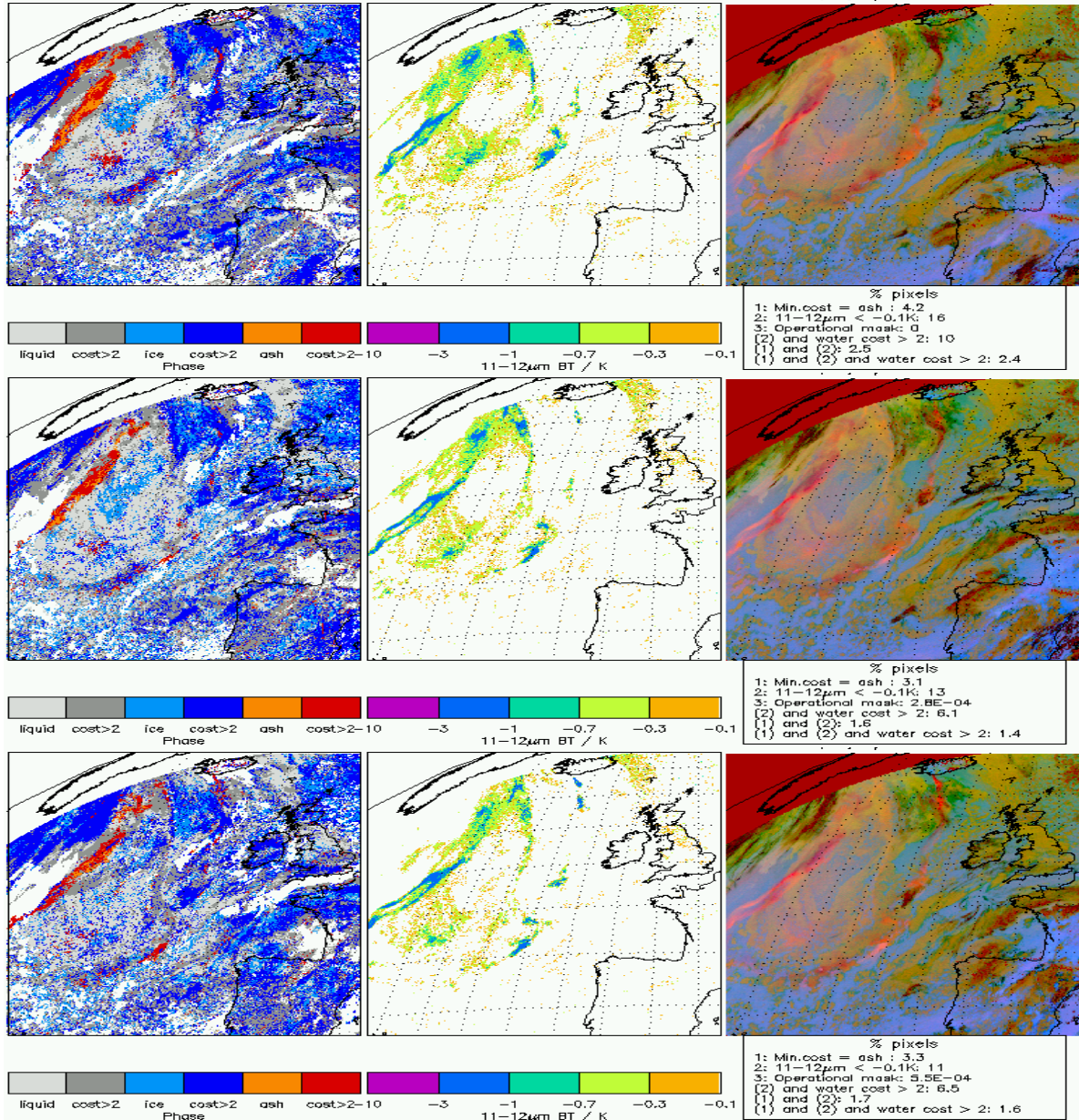
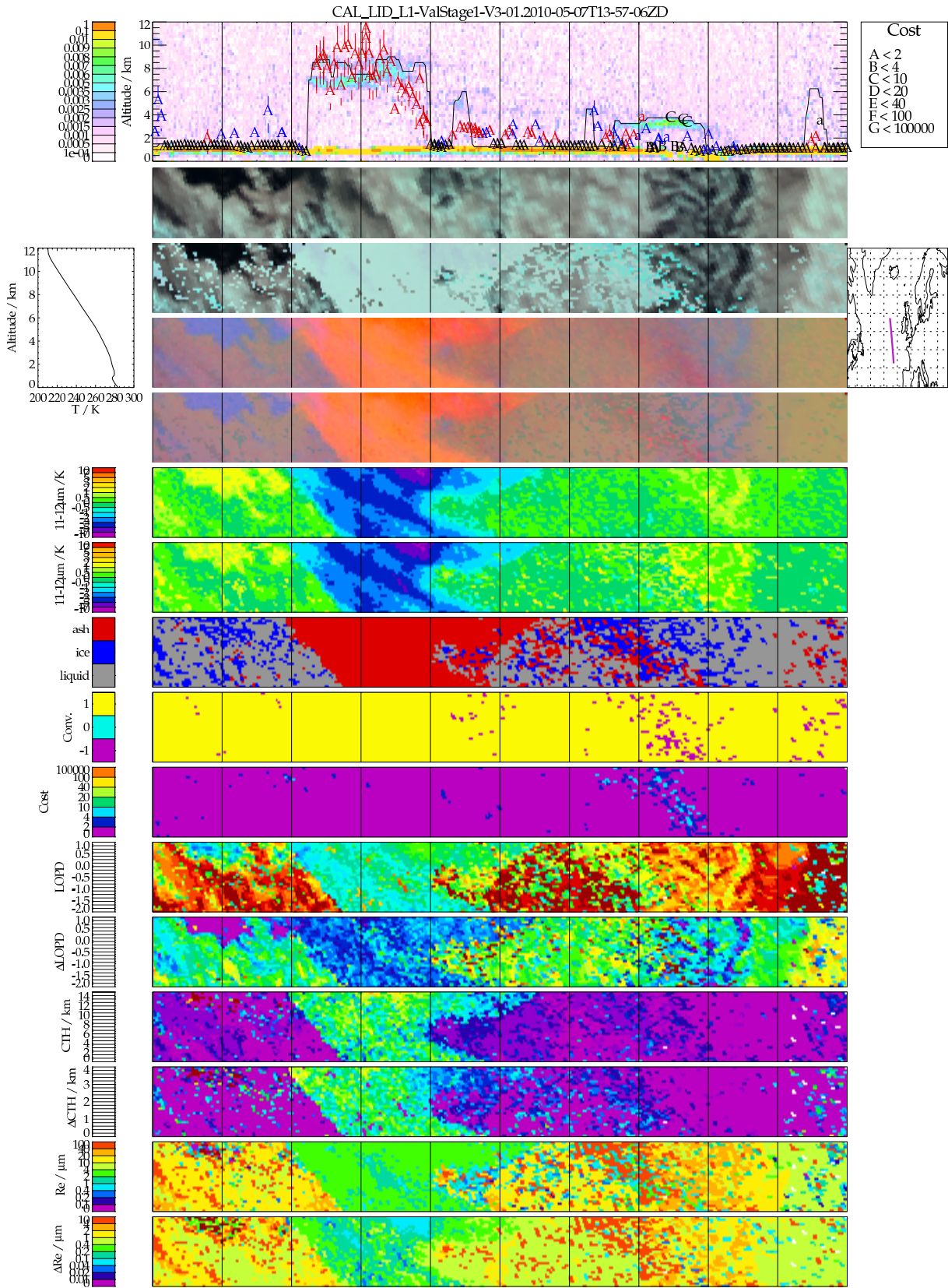


Figure 13: Cloud type, 11-12 μm brightness temperature difference and 8.7, 11, 12 μm false colour image for 9:12, 12:12, 15:12 and 18:12 UT on 10 May 2010.



112322/02/11. two_MSG2-SEVI-MSG15-0100-NA-20100507144241.667000000Z-995378_awat2_ash_cal_spi_zstar_v2p11_45_55_0

Figure 14c: Two-layer retrieval at 14:42 on 7 May 2010. Loose fit to water-vapour channels.

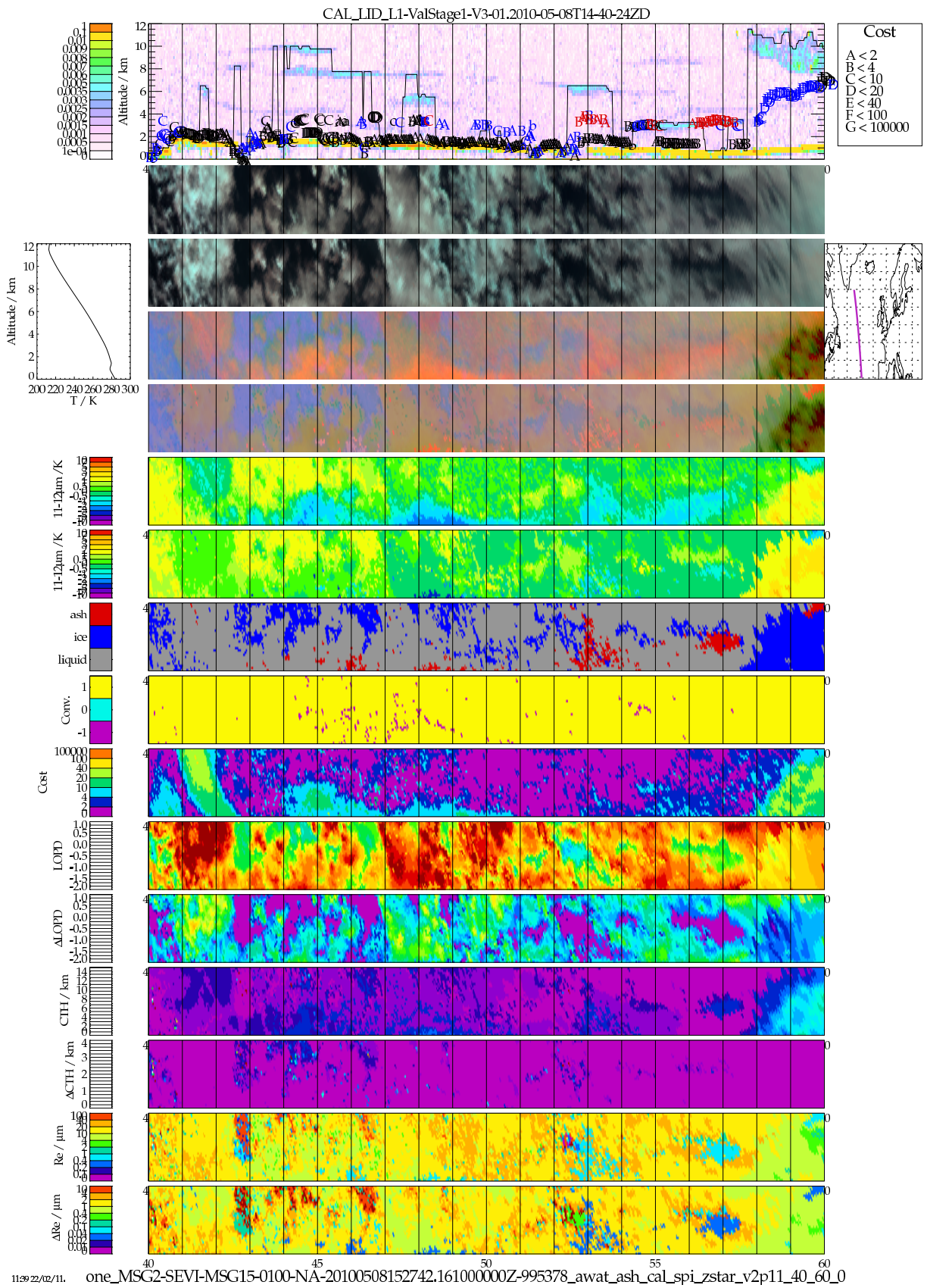


Figure 15a: Single-layer retrieval at 15:27 on 8 May 2010.

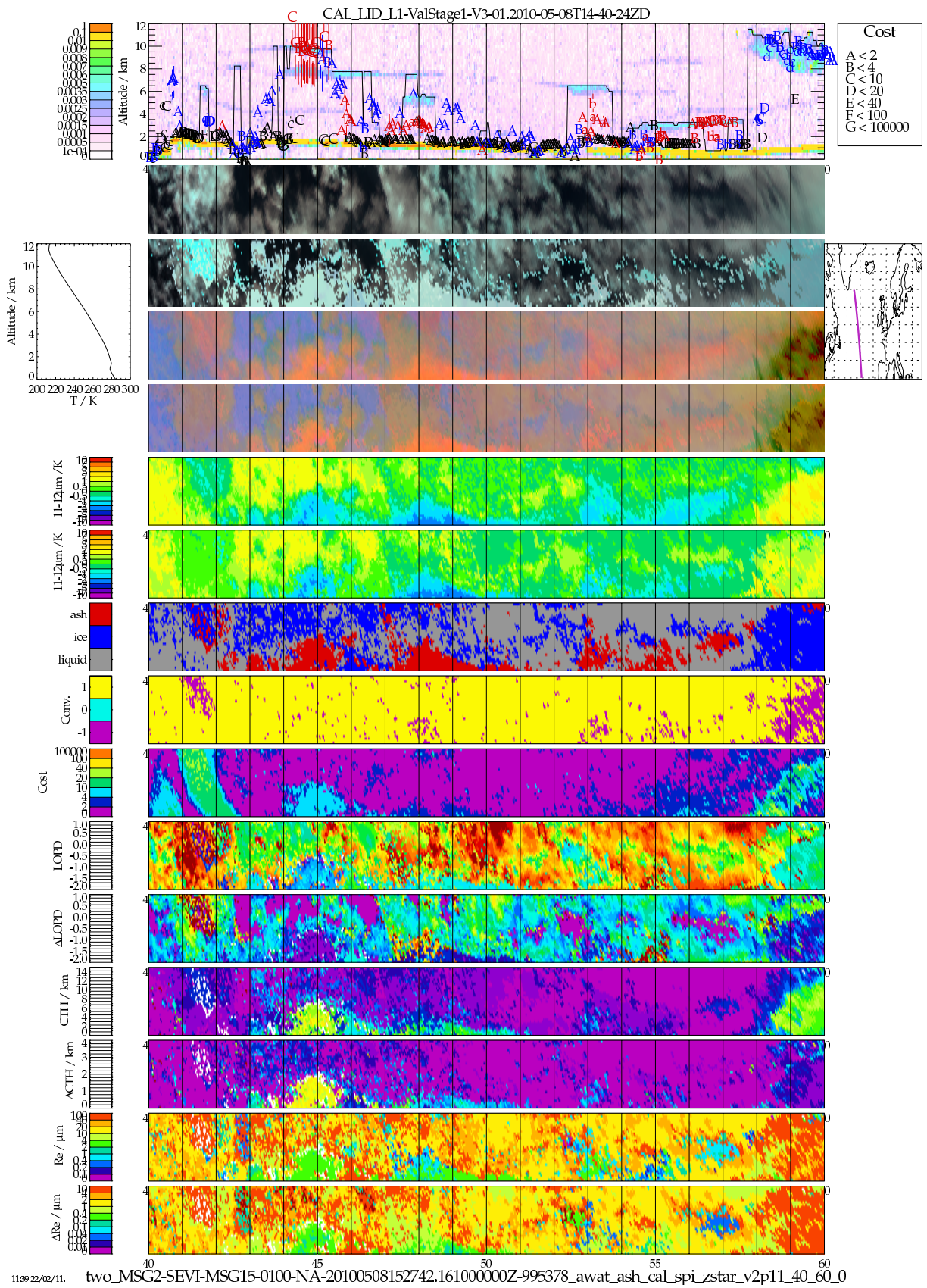


Figure 15b: Two-layer retrieval at 15:27 on 8 May 2010.

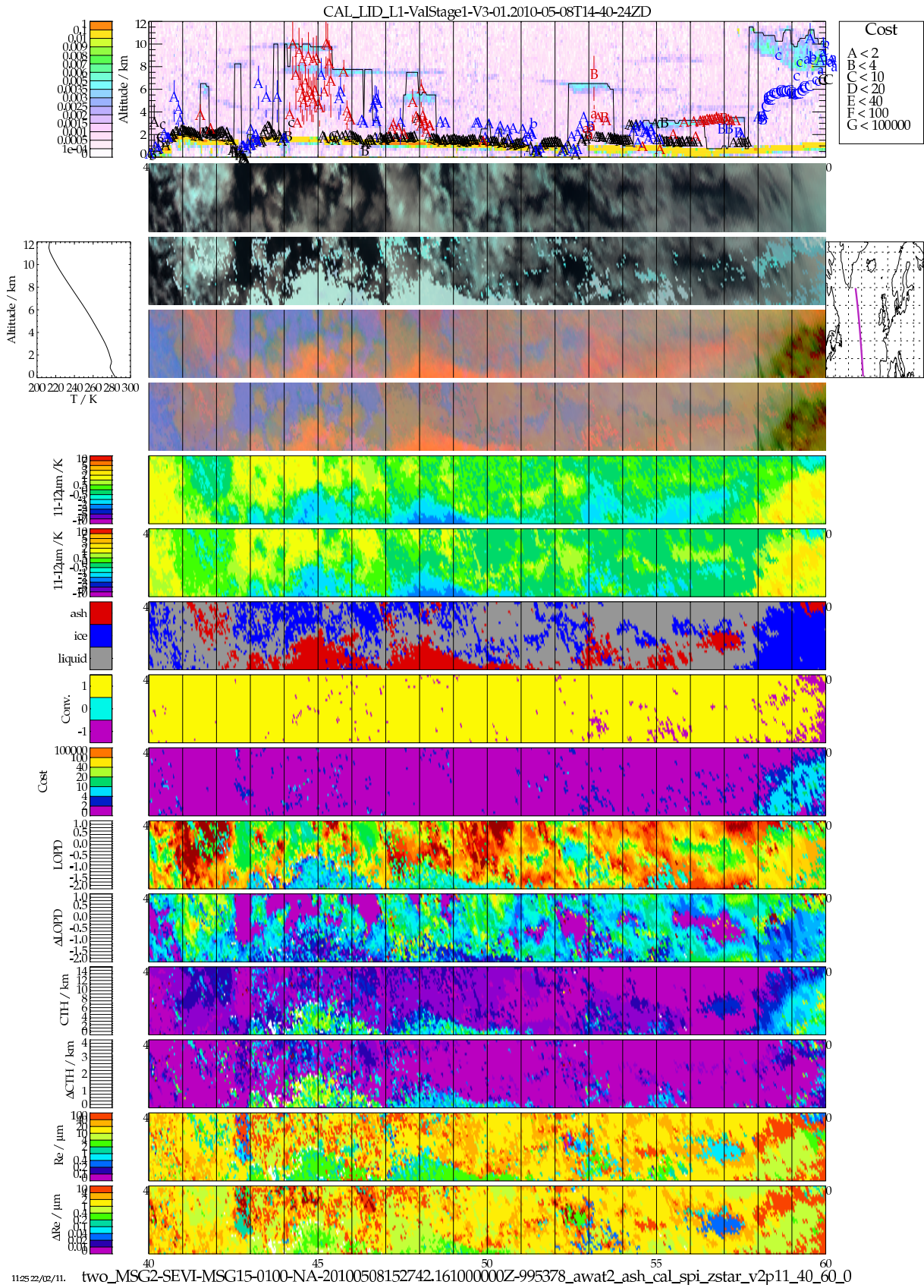


Figure 15c: Two-layer retrieval at 15:27 on 8 May 2010. Loose fit to water-vapour channels.

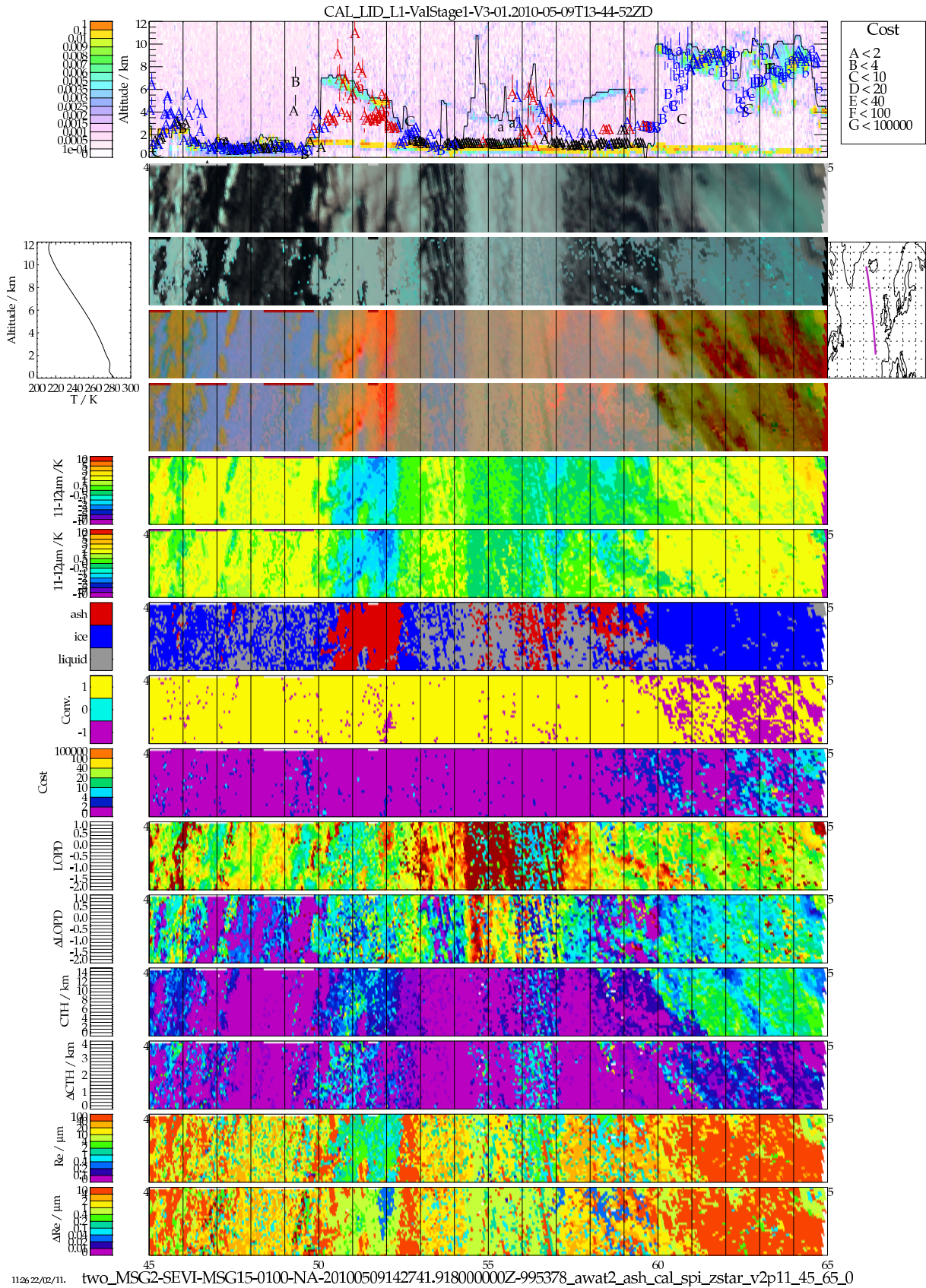


Figure 16c: Two-layer retrieval at 14:27 on 9 May 2010. Loose fit to water-vapour channels.

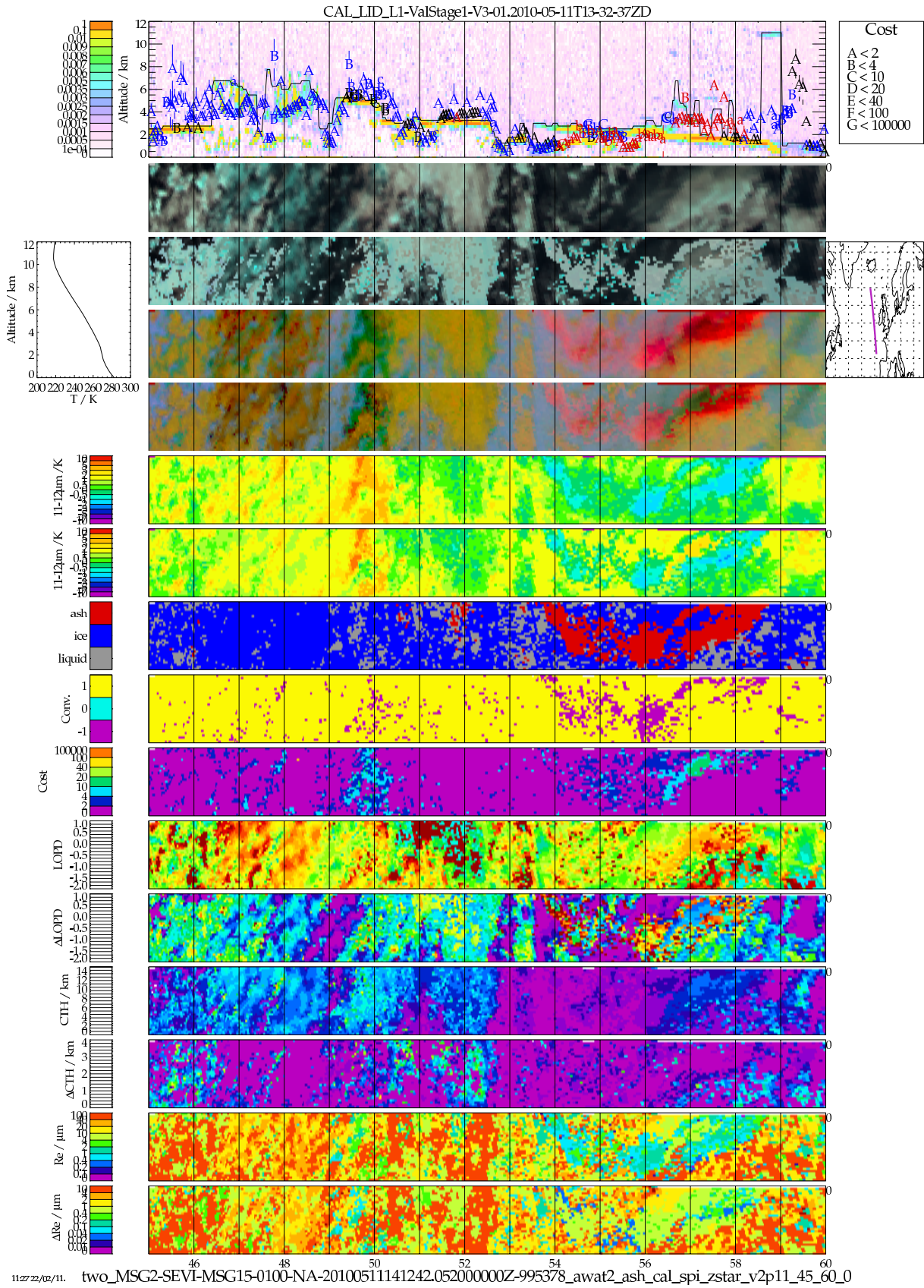


Figure 17c: Two-layer retrieval at 14:12 on 11 May 2010. Loose fit to water-vapour channels.

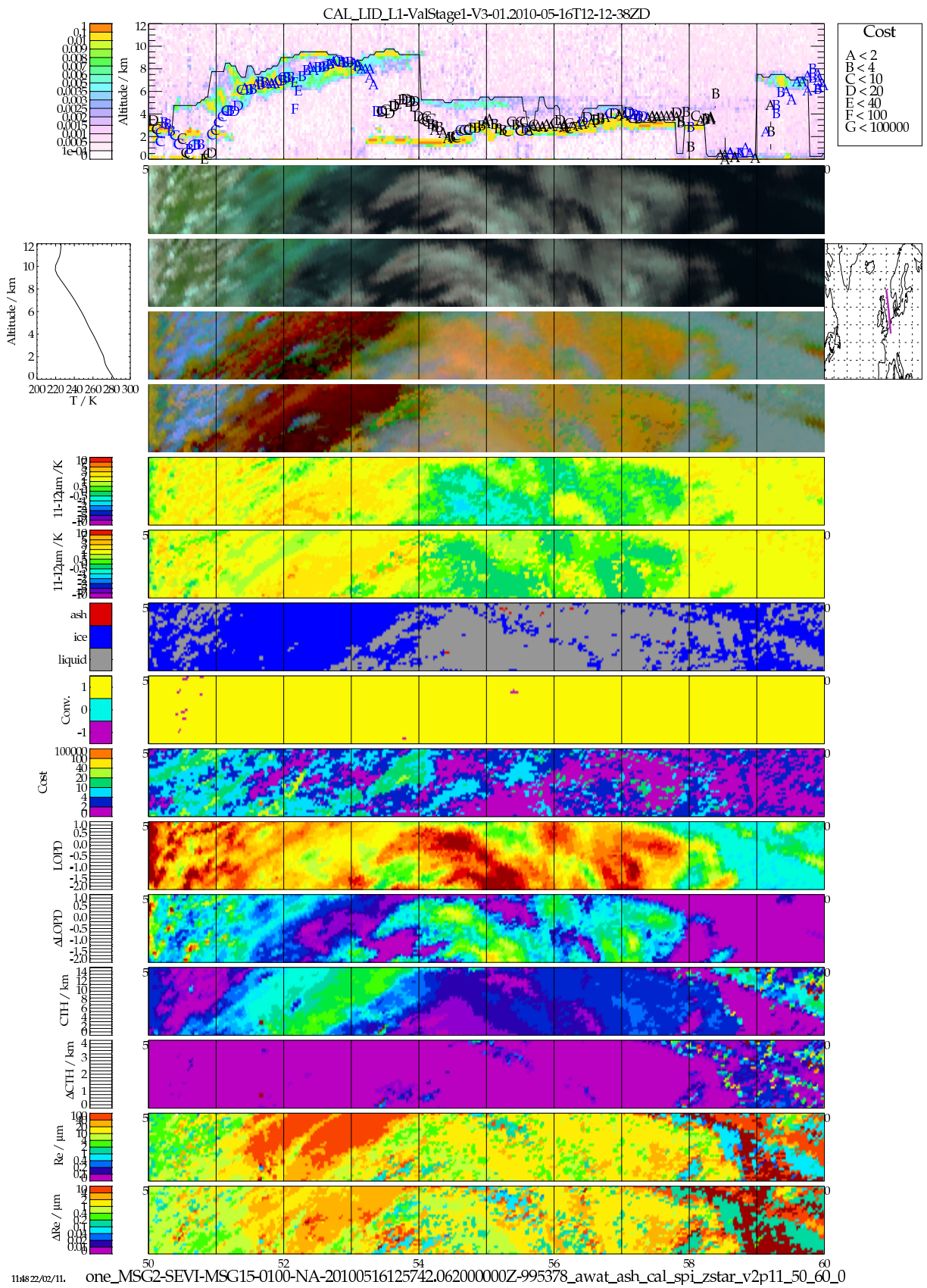


Figure 18a: Single-layer retrieval at 12:57 on 16 May 2010.

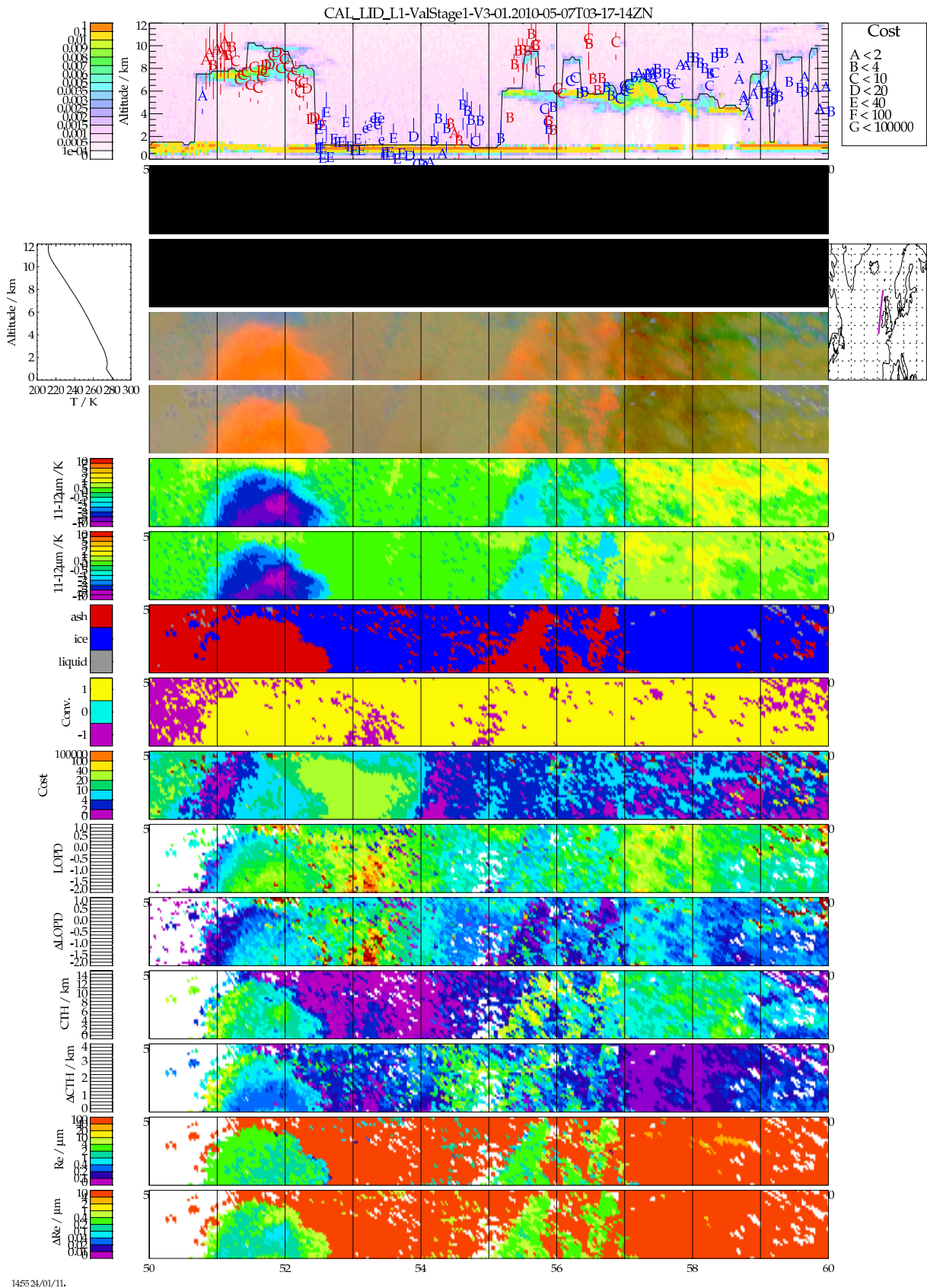


Figure 19a: Two-layer IR only retrieval at 03:27 on 7 May 2010.

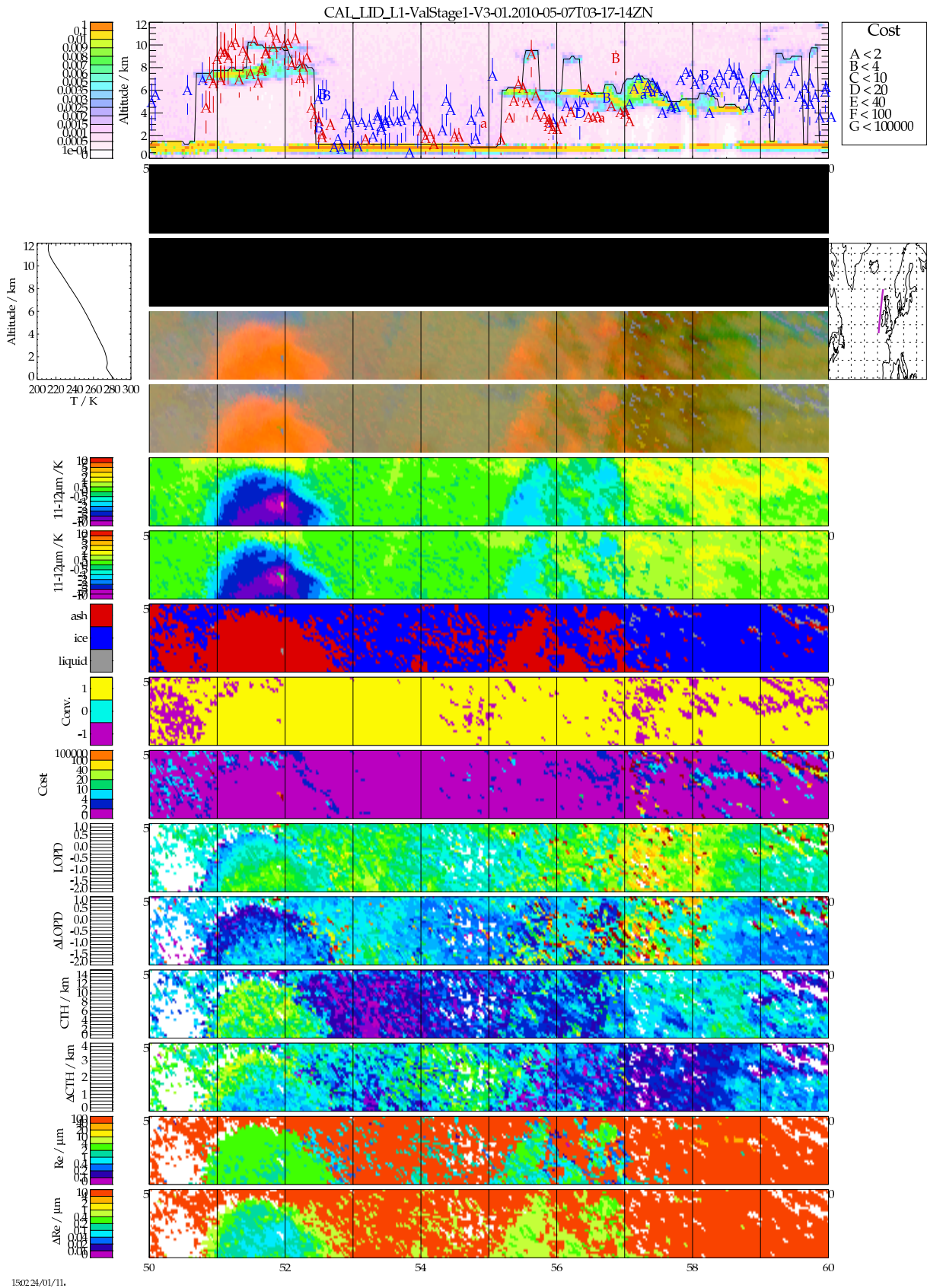


Figure 19b: Two-layer IR only retrieval at 03:27 on 7 May 2010. Loose fit to water-vapour channels.

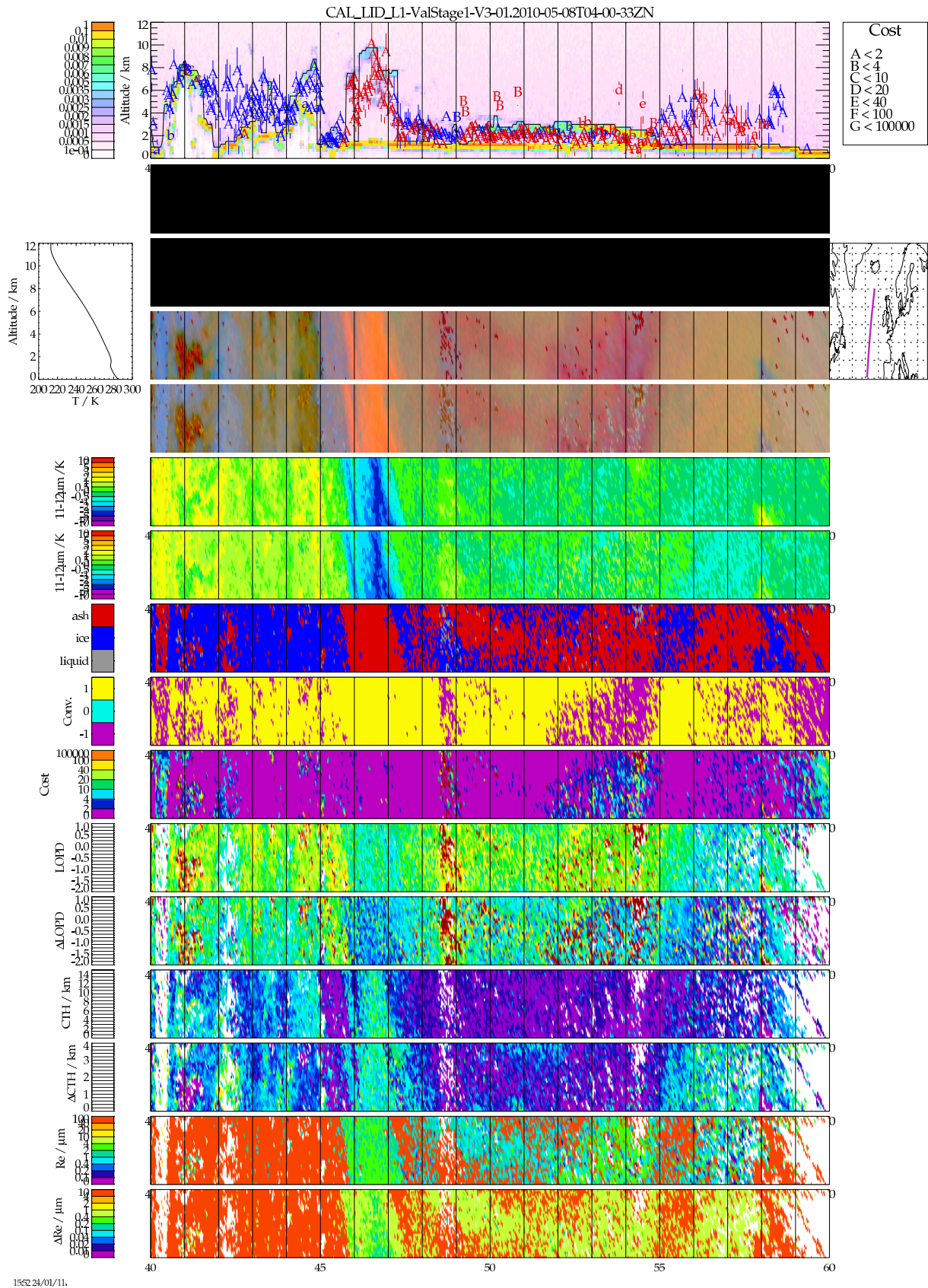


Figure 20b: Two-layer IR only retrieval at 04:12 on 8 May 2010. Loose fit to water-vapour channels.

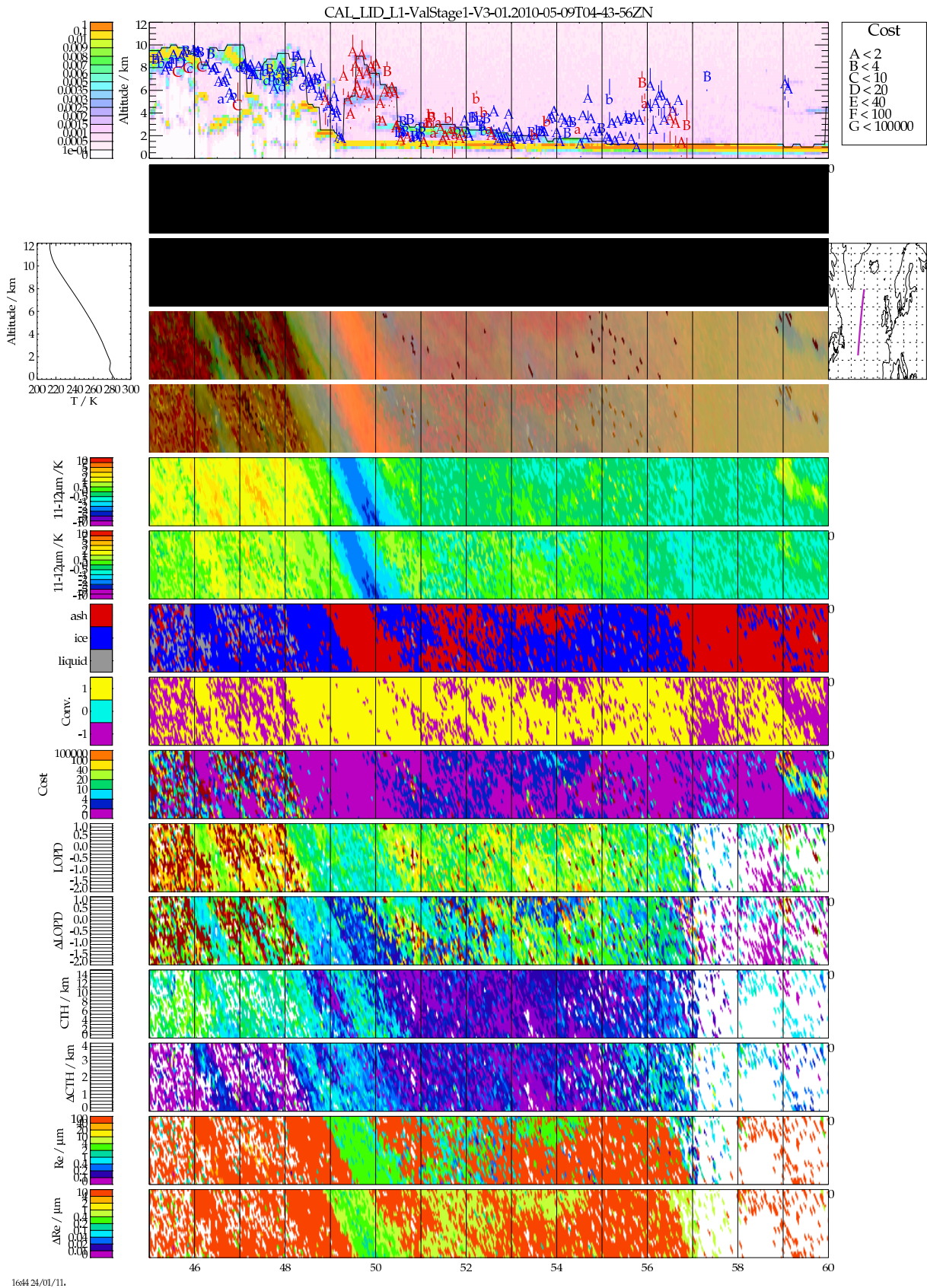


Figure 21b: Two-layer IR only retrieval at 05:12 on 9 May 2010. Loose fit to water-vapour channels.

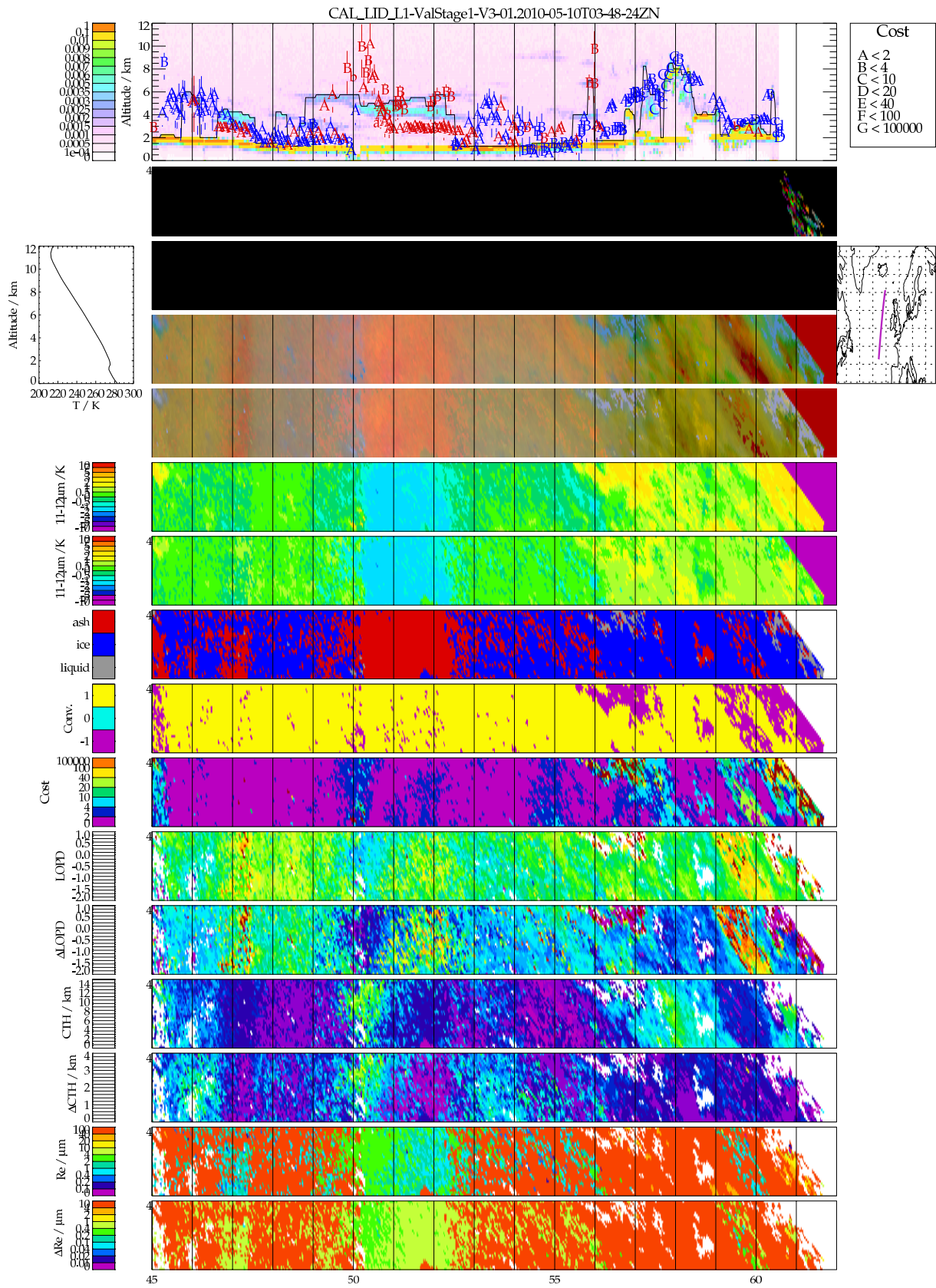


Figure 22a: Two-layer IR only retrieval at 03:57 on 10 May 2010.

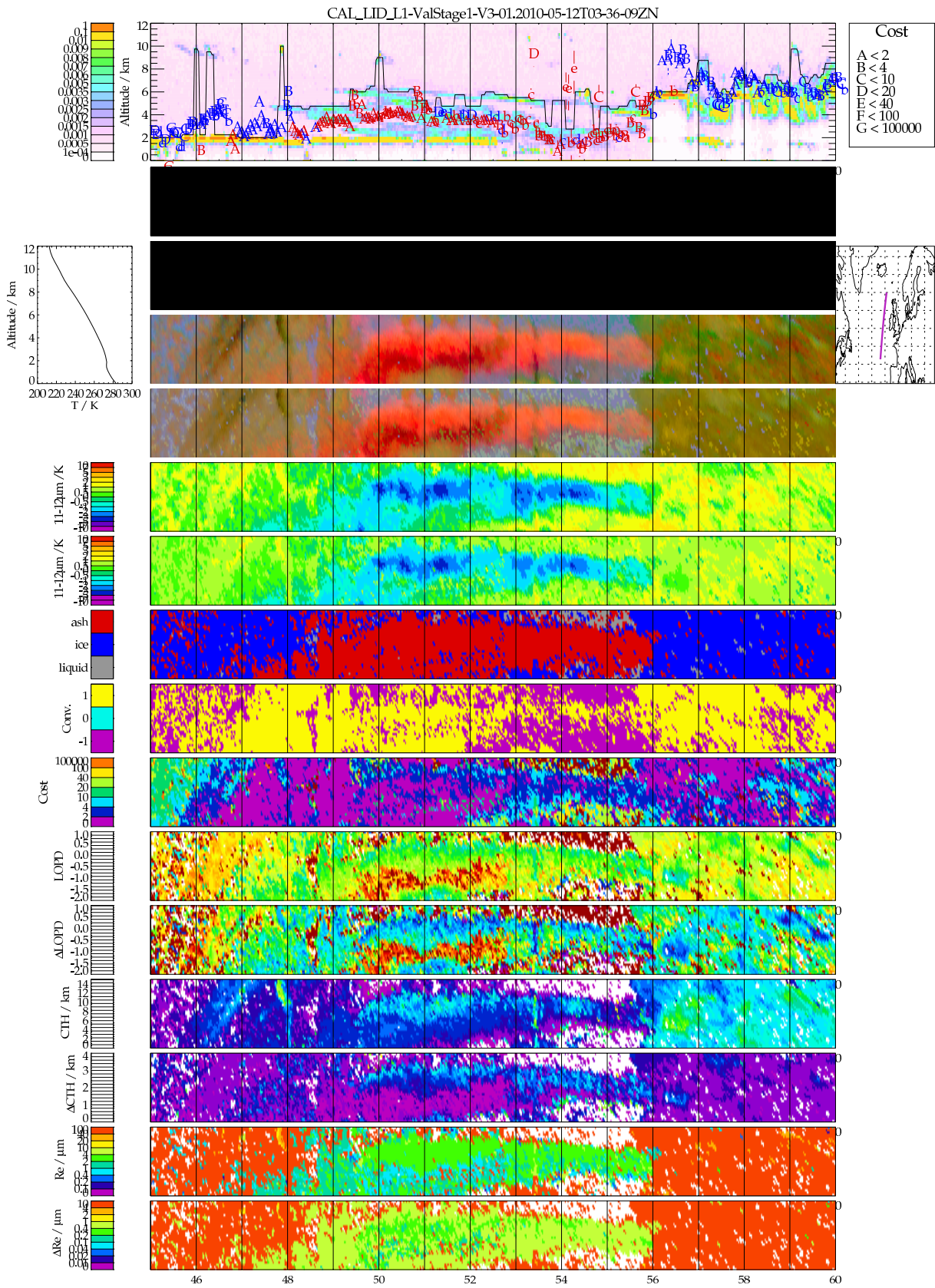


Figure 23a: Two-layer IR only retrieval at 03:42 on 12 May 2010.

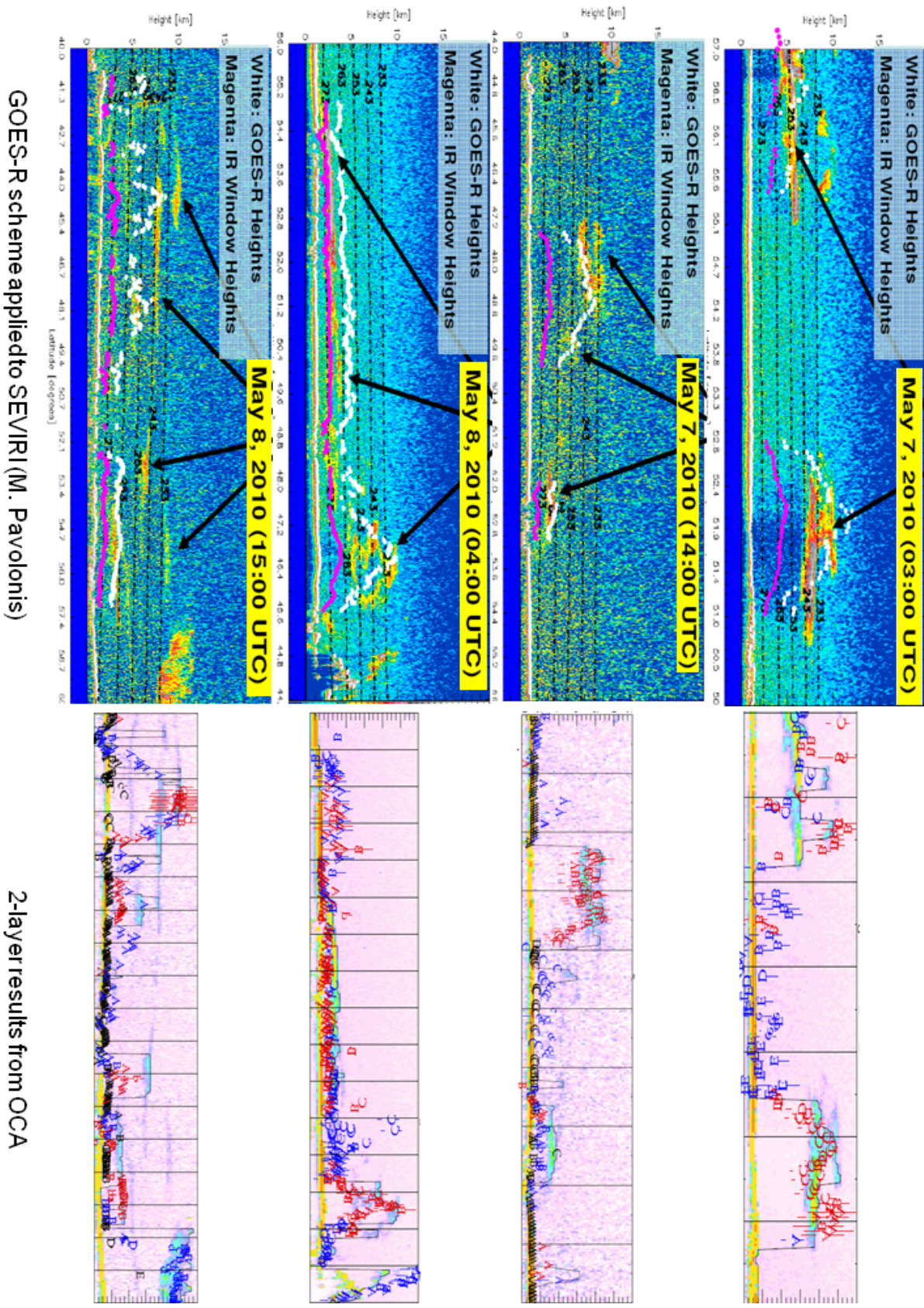


Figure 25: Comparison of OCA results (right) to those produced by M. Pavolonis by applying the GOES-R scheme to SEVIRI (left).